IOP Publishing Journal of Neural Engineering

J. Neural Eng. **4** (2007) 294–308 doi:10.1088/1741-2560/4/3/015

Region-specific network plasticity in simulated and living cortical networks: comparison of the center of activity trajectory (CAT) with other statistics

Zenas C Chao, Douglas J Bakkum and Steve M Potter

Laboratory for Neuroengineering, Department of Biomedical Engineering, Georgia Institute of Technology and Emory University School of Medicine, Atlanta, GA 30332-0535, USA

E-mail: steve.potter@bme.gatech.edu

Received 15 January 2007
Accepted for publication 8 June 2007
Published 6 July 2007
Online at stacks.iop.org/JNE/4/294

Abstract

Electrically interfaced cortical networks cultured *in vitro* can be used as a model for studying the network mechanisms of learning and memory. Lasting changes in functional connectivity have been difficult to detect with extracellular multi-electrode arrays using standard firing rate statistics. We used both simulated and living networks to compare the ability of various statistics to quantify functional plasticity at the network level. Using a simulated integrate-and-fire neural network, we compared five established statistical methods to one of our own design, called center of activity trajectory (CAT). CAT, which depicts dynamics of the location-weighted average of spatiotemporal patterns of action potentials across the physical space of the neuronal circuitry, was the most sensitive statistic for detecting tetanus-induced plasticity in both simulated and living networks. By reducing the dimensionality of multi-unit data while still including spatial information, CAT allows efficient real-time computation of spatiotemporal activity patterns. Thus, CAT will be useful for studies *in vivo* or *in vitro* in which the locations of recording sites on multi-electrode probes are important.

M This article features online multimedia enhancements

(Some figures in this article are in colour only in the electronic version)

Introduction

Modification of connectivity between cortical neurons plays an important role in the processes of learning (Ahissar *et al* 1992, Buonomano 1998) and memory (Merzenich and Sameshima 1993). Connectivity at the synaptic level has been studied by administering stimuli while simultaneously recording neural activity, and then quantifying plasticity by analyzing the stimulus–response relationships. Culturing on multi-electrode arrays (MEAs) (figures 1(a) and (b)) was introduced to help understand connectivity and plasticity in networks of neurons (Gross 1979, Pine 1980). This allows long-term (months), non-invasive observation of the electrical activity of multiple neurons simultaneously (Potter and DeMarse 2001) in a system with less experimental complexity and greater control than preparations *in vivo*. External factors such as sensory inputs, attention and behavioral drives are absent, while many aspects of complex spatiotemporal spike patterns observed in animals remain (Gross and Kowalski 1999, Shefi *et al* 2002).

Many activity statistics have been used to quantify stimulus–response relationships from simultaneous recordings of multiple neurons (Brown *et al* 2004). Most analyze the dependences between spike trains, such as the maximum likelihood method (Chornoboy *et al* 1988, Okatan *et al* 2005), product–moment correlation coefficient (Kudrimoti *et al* 1999), functional holography (Baruchi and Ben-Jacob 2004), etc. However, only a few were applied for measuring network plasticity. The most common of these was the firing

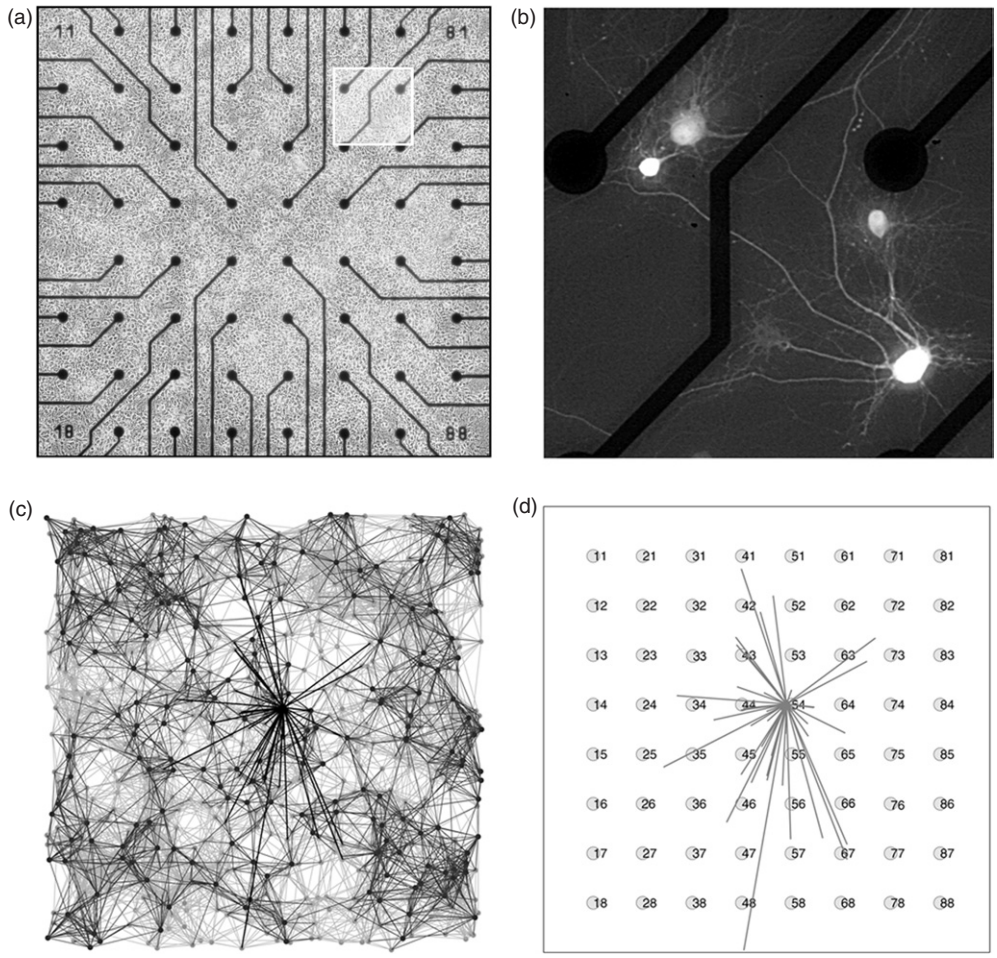

Figure 1. Living MEA culture versus simulated network. The simulated neural network and stimulation electrodes were constructed to mimic the dissociated cultured network and MEA setup. (a) A view of a living MEA culture with 60 electrodes. (b) Neurons, tagged with yellow fluorescent protein, in the highlighted area shown in (a). (c) The structure of a simulated network with 1000 LIF neurons located in a 3 mm by 3 mm region. The circles indicate the neurons, the light-gray lines represent the excitatory synapses and the dark-gray lines represent the inhibitory synapses. All neurons are shown but only 15% of the synaptic connections are shown for clarity. The thick black lines emphasize the connections from a particular randomly selected neuron. (d) The locations of 64 electrodes are shown in circles, and marked with column–row numbers. The connections of the same neuron highlighted in (c) are depicted in light gray.

rate (FR), which showed plastic modifications of network response induced by tetanic stimulation in cortical cultures (Reich *et al* 1997, Jimbo *et al* 1998, Maeda *et al* 1998, Jimbo *et al* 1999, Wagenaar *et al* 2006a) and dopamine-regulated plasticity in anesthetized rats (Rosenkranz and Grace 1999). Firing rate histogram (FRH) uses firing rates integrated over successive sequential latency epochs to add detailed temporal information, and was applied to demonstrate adaptable image processing and pattern recognition through training by tetanic stimulation in MEA cultures (Ruaro *et al* 2005). Mutual information (MI) characterized the statistical dependence between neuron pairs, exposing the strength of coupling between neurons and the functional connectivity among cortical areas (David *et al* 2004). Cross-correlation histograms (CCH) from pairs of neurons showed functional plasticity in the auditory cortex of behaving monkeys (Ahissar *et al* 1998), and the more advanced shift-predictor corrected cross-correlogram (SCCC) was used to quantify receptive field plasticity in the rat auditory cortex (Bao *et al* 2003). Joint peri-stimulus time histogram (JPSTH) characterized the causality of firing between neuron pairs, and successfully demonstrated long-term facilitation of neural activity involved in respiratory control (Morris *et al* 2003). Robust neuronal computation and encoding is believed to involve the distribution of information over populations of neurons and synapses in a combination of spatial and temporal domains. Observing only pairs of neurons (MI, CCH, SCCC and JPSTH), neglecting temporal information (FR) and neglecting spatial information (all) limit the ability of these to measure the complex plasticity of the brain.

We recently devised a statistic called the center of activity trajectory (CAT), which incorporates both the physical locations of the recording sites and the timing of neural activity in order to depict dynamics of the population activity in the *neuronal circuitry space* (Chao *et al* 2005). The neuronal circuitry space is defined by the physical locations of the neurons, in our case being the MEA's two-dimensional plane. The center of activity (CA) component is analogous to the center of mass, in that the 'mass' at an electrode location is determined by the recorded

firing rate. CAT is the sequence of CAs over successive time intervals. We discuss how the inclusion of spatial and temporal information improved the detection of neural network plasticity. The importance of the spatial location of neural activity has been widely emphasized in other studies. For example, spatiotemporal dipole models were used to represent the spatial distribution of underlying focal neural sources producing electroencephalographic (EEG) and magnetoencephalographic (MEG) signals (Scherg 1990, Leahy *et al* 1998).

We used a simulated network to compare CAT's ability to detect network plasticity to the alternative statistics: FR, FRH, MI, SCCC and JPSTH. No ground truth about network plasticity in living networks exists, because neuronal connectivity cannot be measured for more than a few pairs of neurons simultaneously. Therefore, we could only cross-validate the amount of plasticity detected by each statistic in a simulated network, in which the weights of *all* synapses were observable. In simulation, we modulated neural plasticity in a controlled manner, and quantified the ability of each statistic to reveal underlying changes in synaptic connectivity.

In simulation, CAT showed the ability to detect smaller changes in the distribution of network synaptic weights than did FR, FRH, MI, SCCC or JPSTH. CAT also detected more pronounced changes in the network following tetanus than the alternate statistics in living MEA cortical cultures.

By applying a shuffling method to the CAT analysis to erase spatial information about recording location in its calculation, we found that changes in activity patterns recorded from neighboring electrodes were not independent and contributed to the better performance of CAT to detect plasticity. The network plasticity was *region specific*: despite the apparent random connectivity of neurons, plasticity was not symmetrically distributed, and the location of neurons played a role in stimulus-induced plasticity.

Methods

Simulation

Simulated networks. We used the Neural Circuit SIMulator (Natschlager *et al* 2002) to produce five artificial neural networks, as described previously (Chao *et al* 2005) (also see supplemental materials 1 available at stacks.iop.org/JNE/4/294). Briefly, 1000 leaky-integrate-and-fire (LIF) model neurons, with a total of 50 000 synapses, were placed randomly in a 3 mm by 3 mm area (see figure 1(c)). All synapses were frequency dependent (Markram *et al* 1998, Izhikevich *et al* 2004) to model synaptic depression. 70% of the neurons were excitatory, with spike-timing-dependent plasticity (STDP) (Song *et al* 2000). We included an 8 by 8 grid of electrodes; 60 of these were used for recording and stimulation as in a real MEA (four excluded electrodes were corner electrodes 11, 18, 81 and 88, see figure 1(d)).

Setup of networks with different synaptic states. The *synaptic state* of a network was determined by its connections and synaptic weight distribution. In order to generate different synaptic states, we used five networks with different connectivity as reference networks. We ran the networks for 5 h in simulated time until the synaptic weights reached a steady state (see supplemental materials 1 available at stacks.iop.org/JNE/4/294). The set of synaptic weights stabilized after 5 h of spontaneous activity, without external stimuli, and was used as the initial state for the corresponding reference network.

For each reference network, we applied simulated tetanization at two randomly picked electrodes at 20 Hz, and a series of subsequent networks (different synaptic states) were collected after different tetanus durations (1, 2, 5, 10, 15, 20, 30 s and 1, 2, 5 min). That is, starting from a reference network (S_0), S_1 was the network with the synaptic state at 1 s after the start of tetanization, S_2 at 2 s, and so forth. Therefore, for each pair of randomly chosen tetanization electrodes, ten new networks with different synaptic states were obtained. This process was repeated for each reference state using ten different tetanization electrode pairs. By altering the five reference networks in this manner, a total of 500 new networks with different synaptic states were obtained.

Tetanic stimulation induces long-lasting changes in synaptic transmission (Bliss and Lømo 1973), which shapes how neural circuits process information and is involved in behavioral modifications, including simple forms of learning in motor control (Fisher *et al* 1997). Administration of 20 Hz tetanization, as in our study, was widely used to induce long-term facilitation (LTF) of post-synaptic potentials at crayfish neuromuscular junctions (Wojtowicz and Atwood 1985, Delaney *et al* 1989), short-term synaptic plasticity in anesthetized fish (Fortune and Rose 2000), long-term potentiation (LTP) in hippocampal slices (Miles and Wong 1987) and modification of synaptic strength in cortical cultures (Jimbo *et al* 1999). In our simulated networks, tetanization induced both LTP and long-term depression (LTD) of synapses through STDP: firing of a post-synaptic neuron immediately after a pre-synaptic neuron results in LTP of synaptic transmission and the reverse order of firing results in LTD (Levy and Steward 1983, Markram *et al* 1998, Bi and Poo 1998, Gerstner *et al* 1996).

Simulations with random probing sequence (RPS). For each network, we ran ten simulations with different 10 min random probing sequences (RPSs). Therefore, a total of 5050 simulations were performed separately on 505 networks (500 new networks and 5 reference networks). The probe stimuli were applied to all 60 electrodes, one at a time, with inter-stimulus intervals on a given electrode drawn from independent exponential distributions with a mean of 60 s. Thus, each electrode stimulated the simulated network with different random sequences, averaging 1 pulse per second for the whole array.

In each simulation, there were 10.0 ± 3.1 (mean and standard deviation) stimuli delivered at each electrode. The same Gaussian noise, introduced into neurons as fluctuations in membrane voltage, was used for each simulation to control the effects of self-firing or of sub-threshold fluctuation of membrane potential on activity. In order to ensure that the

statistics calculated from the same network correspond to the same synaptic state, the STDP algorithm was turned off throughout the simulation to prevent ongoing activity changing the network state.

Plasticity statistics. Five commonly used statistics and the center of activity trajectory (CAT) were measured from each simulation (see figure 7). The five commonly used statistics were FR, FRH, mutual information (MI), SCCC and JPSTH (see supplemental materials 2 available at stacks.iop.org/JNE/4/294).

Center of activity trajectory (CAT). CAT represents spatiotemporal patterns of network-wide population activity. As applied here, it is a spatially weighted measure of temporally binned responses to single-electrode stimuli in neuronal circuitry space. During each simulation, stimuli at each electrode occurred multiple times (10.0 ± 3.1 times) in one RPS. FRH from the recording electrode E_k to the stimulus at electrode P_i, $\mathrm{FRH}_{E_k}^{P_i}$, was defined as the average number of spikes counted in a 5 ms moving time bin with 500 μs time step over trials. $\mathrm{FRH}_{E_k}^{P_i}(n)$ represents the value of $\mathrm{FRH}_{E_k}^{P_i}$ in the nth bin, and $\mathrm{Col}(E_k)$ and $\mathrm{Row}(E_k)$ are the column number and the row number of the electrode E_k, respectively. For example, the electrode in column number 2 and row number 8 is 28 (see figure 1(d)). The value of CA in the nth bin for the stimulation electrode P_i has X and Y components, which are defined as

$$\left[\mathrm{CA}_X^{P_i}(n), \mathrm{CA}_Y^{P_i}(n)\right] = \frac{\sum_{k=1}^{60} \mathrm{FRH}_{E_k}^{P_i}(n)[\mathrm{Col}(E_k) - R_{\mathrm{col}}, \mathrm{Row}(E_k) - R_{\mathrm{row}}]}{\sum_{k=1}^{60} \mathrm{FRH}_{E_k}^{P_i}}, \quad (1)$$

where R_{col} and R_{row} are the coordinates of a reference point (the physical center of the 8 by 8 grid of electrodes, in our case). CA was calculated with an electrode number in the neuronal circuitry space, which is equivalent to using the physical location since the inter-electrode spacing is constant. The corresponding X and Y components for CAT are defined as

$$\mathrm{CAT}_X^{P_i} = \left[\mathrm{CA}_X^{P_i}(1), \mathrm{CA}_X^{P_i}(2), \ldots, \mathrm{CA}_X^{P_i}(n), \ldots, \mathrm{CA}_X^{P_i}(N)\right]$$
$$\mathrm{CAT}_Y^{P_i} = \left[\mathrm{CA}_Y^{P_i}(1), \mathrm{CA}_Y^{P_i}(2), \ldots, \mathrm{CA}_Y^{P_i}(n), \ldots, \mathrm{CA}_Y^{P_i}(N)\right], \quad (2)$$

where N is the total number of bins in $\mathrm{FRH}_{E_k}^{P_i}$. Intuitively, CA is analogous to the center of mass, where the 'mass' at an electrode location is determined by the recorded FR. CAT is the sequence of CAs over successive time intervals.

CA reflects spatial asymmetry of neural activity about the reference point (the center of the dish), and CAT represents the dynamics of CA. That is, if the network is firing symmetrically, the CA will be at the center of the dish, whereas if the network fires mainly in one corner then the CA will be found off-center toward that corner. CA reduces the dimensionality from 60 to 2, and it is not an injective (information-preserving) function of activity distribution. See supplemental materials 3 (available at stacks.iop.org/JNE/4/294) for CAT in a simulated network, and Supplemental Materials 5 (available at stacks.iop.org/JNE/4/294) for CAT in an MEA culture.

Evaluating the performances of different statistics. Performance of a statistic was defined by the smallest change in network synaptic weights that could be detected as significant. To evaluate performance in each simulation, we evaluated the statistic for evoked responses to all 60 stimulation electrodes and joined these together into a large vector representing the whole stimulus–response information (input–output function) of the network. We called this joint vector the whole-input–output (WIO) vector of the statistic. Figure 2 demonstrates the calculation of the WIO vector for CAT. A visualization of the change in WIO vectors for CAT from S_0 to S_1–S_{10} appears in figure 3.

We measured the Euclidian distances $E(S_i)$ between ten WIO vectors (from ten simulations with different RPSs) calculated at S_i to the centroid calculated at S_0 (shown as a cross in figure 3). We then compared $E(S_i)$ for S_1–S_{10} to $E(S_0)$ separately, and the p-values ($n = 10$ RPSs, Wilcoxon signed rank test, which tests the magnitudes of the differences between paired observations without assumptions about the form of the distribution of the measurements) were computed to quantify the significance of differences. For each state, the relation between the mean p-values ($n = 50$, from five reference networks and ten tetanization electrode pairs per reference network) and the mean absolute synaptic change (MASC) was quantified

$$\mathrm{MASC}(S_i) = \frac{1}{N}\sum_{k=1}^{N} \frac{\|W_k(S_i) - W_k(S_0)\|}{0.5} \times 100\%, \quad (3)$$

where N is the number of excitatory synapses and $W_k(S_i)$ represents the synaptic weight of the kth excitatory synapse at network S_i. We normalized the absolute change in each synapse by the possible range, 0 to 0.5, for excitatory synapses. We determined the performance of different statistics as the minimum MASC for p-values below a significance threshold of 0.05; this is termed 'detectable MASC'. The smaller the MASC a statistic can detect, the better the statistic's performance.

Evaluation of the sensitivities and specificities of different statistics. Successful performance can be artificially enhanced if a statistic mistakes some non-significant changes as being significant. Therefore, analyzing sensitivity (ability to detect significant plasticity) and specificity (ability to discount insignificant plasticity) can further determine the quality of a statistic. *Sensitivity* was defined as the probability that a statistic indicated a significant difference when calculated from two significantly different network synaptic states (probability of a true positive). *Specificity* was defined as the probability that a statistic showed no significant difference when calculated from networks with no significant difference in synaptic state (probability of a true negative). Together, sensitivity and specificity described the accuracy of a statistic.

For each reference network, the 500 new states (S_1 to S_{10}) were individually evaluated to determine whether their synaptic weight distributions were significantly different from the distribution of the reference state (two-sample Kolmogorov–Smirnov test, which tests whether the two samples have the same distribution, two-tailed, $\alpha = 0.05$). If a

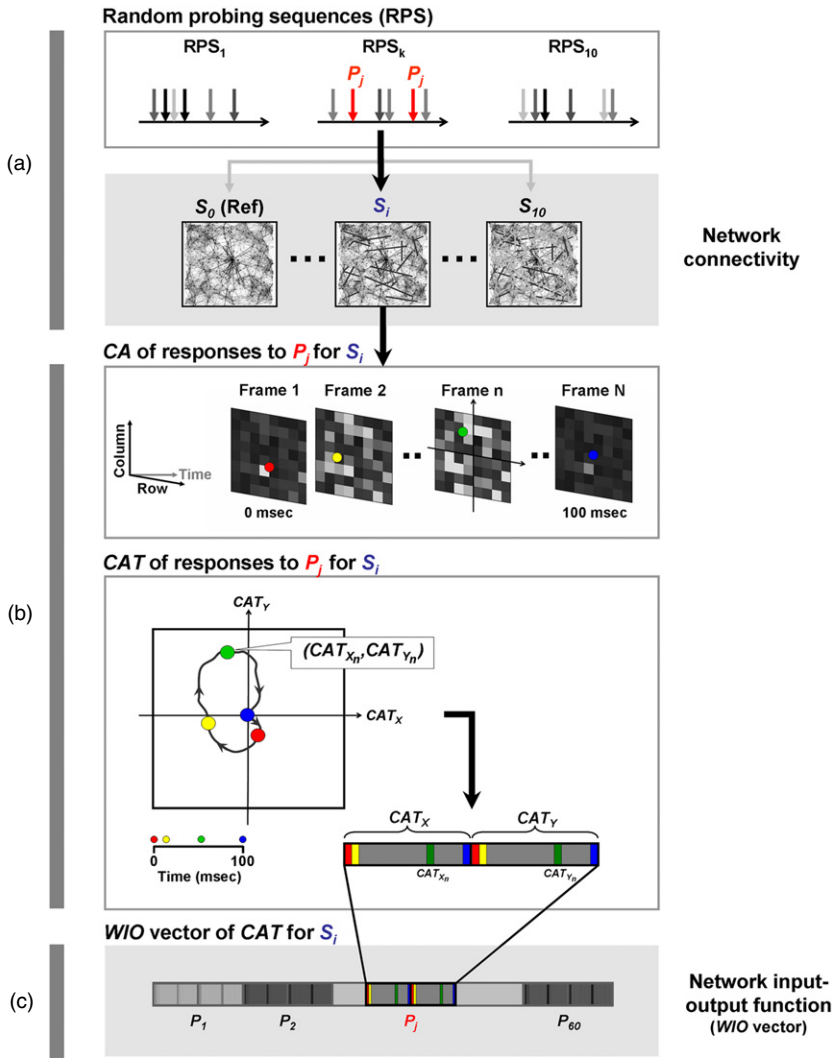

Figure 2. Whole-input–output (WIO) vectors for analyzing performances of different statistics. WIO vectors calculated from each statistic were used to represent the network input–output function. As an example, the WIO vector of CAT calculated from probe responses to one RPS at one network state is demonstrated. (a) An RPS, RPS_k, was delivered into a network with the synaptic state S_i. (b) CA was calculated for evoked responses to the stimulation electrode P_j ($j = 1$ to 60). Each frame indicates the firing rate over a 5 ms moving time window (with a 500 μs time step) on an 8 by 8 grid of electrodes averaged over multiple stimuli at P_j (RPS_k might have multiple stimuli delivered at P_j, see (a)). The 2D trajectory of CAs from frame 1 to frame N (from 0 to 100 ms after the stimuli), CAT, can be represented by a 1D vector by joining CAT_X and CAT_Y. This vector represents CAT of responses to stimuli P_j at the network state S_i. (c) CATs for responses to 60 different stimulation electrodes (P_1 to P_{60}) were joined together to form the WIO vector. This WIO vector represents the input–output function, in terms of CAT, of the network state S_i. For each statistic, each synaptic state has one corresponding WIO vector to describe its input–output function. The statistic that is sensitive to changes in network synaptic states should be able to show significantly different WIO vectors from different synaptic states. One WIO vector was constructed for each RPS (RPS_k, $k = 1$ to10) in each network state (S_i, $i = 0$ to 10). Therefore, for each statistic, 5050 WIO vectors were obtained (=(500 + 5) × 10. 505: 500 new networks + 5 reference networks, 10: number of RPSs delivered to each network).

statistic showed a significant difference (p-value < 0.05; see the previous section) for a state that was significantly different than the reference state (according to the Kolmogorov–Smirnov test), then the result was classified as being a true positive (TP). Conversely, if it showed no significance, then the result was considered a false negative (FN). If a statistic showed significance when calculated from a state that was not significantly different than the reference state, then the result was considered a false positive (FP). If it showed no significance, then the result was considered a true negative (TN). The numbers of TP, FN, FP, and TN were counted for the 500 new networks, and the sensitivity and specificity were defined as

$$\text{Sensitivity} = \frac{\text{TP}}{\text{TP} + \text{FN}} \times 100\%, \qquad \text{Specificity} = \frac{\text{TN}}{\text{FP} + \text{TN}} \times 100\%. \tag{4}$$

Experiments in living cultures

Culture and experimental protocol. Dense networks of dissociated cortical neurons were prepared and cultured as described in Potter and DeMarse (2001). Briefly, embryonic rat cortices were dissected and dissociated using papain and trituration. Fifty thousand cells (~7000 cells mm^{-2})

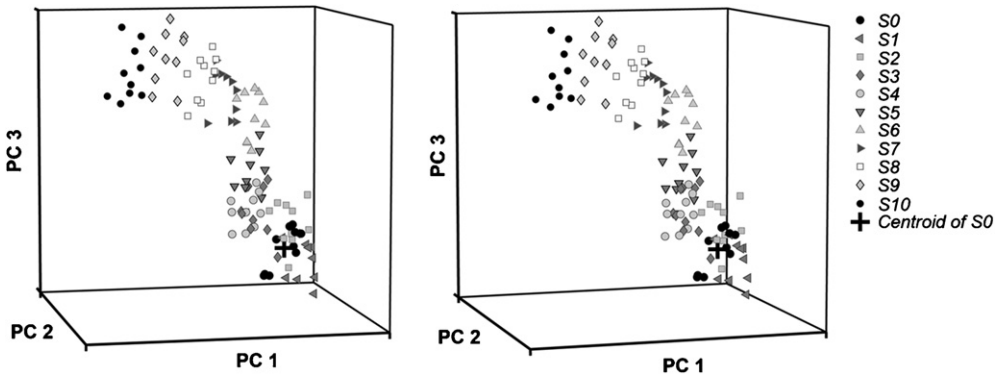

Figure 3. Multi-dimensional whole-input–output (WIO) vectors measured in different synaptic states in simulated networks. The WIO vectors measured from different synaptic states were different. This is a cross-viewing 3D stereogram of an example of the WIO vectors for CATs from the simulations at S_0 to S_{10} (generated by the same tetanization electrodes). Principal components analysis (PCA) was applied on the WIO vectors to visualize the data. Each symbol represents the first three principal components (PC1–PC3) of the WIO vector of a CAT from one simulation. Each synaptic state S_i has ten corresponding symbols, which represent the results from ten different simulations (with different RPSs). The distance of each symbol from the centroid of S_0 (shown as a cross) indicates the amount of change in CATs between the corresponding synaptic state and the reference state. CATs obtained from the synaptic states generated by longer tetanizations were further from CATs obtained from S_0 than those from shorter tetanizations, indicating that longer tetani cause greater plasticity.

were plated on multi-electrode arrays (MultiChannel Systems, Reutlingen, Germany) pre-coated with poly-ethylene-imine (PEI) and laminin. Cultures were grown in Dulbecco's Modified Eagle's Medium (DMEM) containing 10% horse serum.

Six experiments were performed on five cultures from four dissociations. Culture ages ranged from 1 to 3 months (Potter and DeMarse 2001). We delivered biphasic stimuli (monopolar) at 500 mV and 400 μs per phase by using our custom-made stimulator (Wagenaar *et al* 2004, Wagenaar and Potter 2004). Data acquisition, visualization, artifact suppression (Wagenaar and Potter 2002) and spike detection were performed using MultiChannel Systems hardware and our publicly available acquisition and analysis software, Meabench (Potter *et al* 2006). Experiments were conducted in an incubator to control environmental conditions.

Each experiment consisted of a 2 h period of RPS followed by a 15 min tetanic stimulation followed by another 2 h period of RPS (Wagenaar *et al* 2006a). In six experiments, the RPS periods consisted of six electrodes stimulated in a random order at an aggregate frequency of 0.5 Hz (in one experiment, the RPS periods consisted of only four probe electrodes). Fewer electrodes were used in RPS for living networks than simulated networks because not every electrode was able to evoke responses. Two of these electrodes were used for the tetanic stimulation: 150 trains of 20 paired pulse stimuli with 10 ms intervals between paired pulses, 50 ms intervals between pairs and 6 s intervals between the start of each train. Prior to an experiment, every electrode was stimulated in a random order 20 times, and electrodes with six (or four) highest responses (the total number of spikes counted within 100 ms latency after stimuli over recording electrodes) were selected as probe electrodes. The tetanus electrodes were randomly chosen from these.

Measures of CAT, FR, FRH and SCCC. We used evoked responses within 100 ms after the stimuli of RPS for statistics calculations (see supplemental materials 2 available at stacks.iop.org/JNE/4/294). We measured CAT from the evoked responses in the cultured networks and compared it to the three most commonly used statistics: FR, FRH and SCCC. MI was not measured, due to its poor performance in detecting network plasticity in simulations (see results). JPSTH was not measured because of its high dimensionality and computation time (see figure 7 and supplemental materials 2 available at stacks.iop.org/JNE/4/294).

Statistics. For each statistic, we calculated one WIO vector every 240 s (a 'block') for the experiments with six probe stimulation electrodes, and every 160 s for the experiments with four probe stimulation electrodes. Thus, there were 19.9 ± 4.2 (mean and standard deviation) stimuli delivered at each electrode for each WIO vector. Three periods were used for statistics: Pre1, Pre2 and Post1 (see figure 8(a)). Each period had a duration of 52.5 min, and the intervals between Pre1 and Pre2 and between Pre2 and Post1 were 15 min. The 15 min interval between Pre2 and Post1 was the tetanization. For each statistic, the mean distance of the WIO vectors in Pre1 to the centroid of the WIO vectors in Pre2 (C) was compared to the mean distance to their own centroid (D). The ratio of change to drift, C/D, was used to quantify the change from Pre1 to Pre2 before the tetanus (no change if this ratio $\cong$1). A similar measure between Pre2 and Post1 was used to quantify the change across the tetanus. The performance of each statistic to detect the tetanus-induced change was quantified by comparing the two C/Ds ($n = 6$ experiments, Wilcoxon signed rank test).

Results

We tested the performances of six network plasticity statistics in simulated networks: FR, FRH, MI, SCCC, JPSTH and CAT (all acronyms are shown in table 1). We then compared

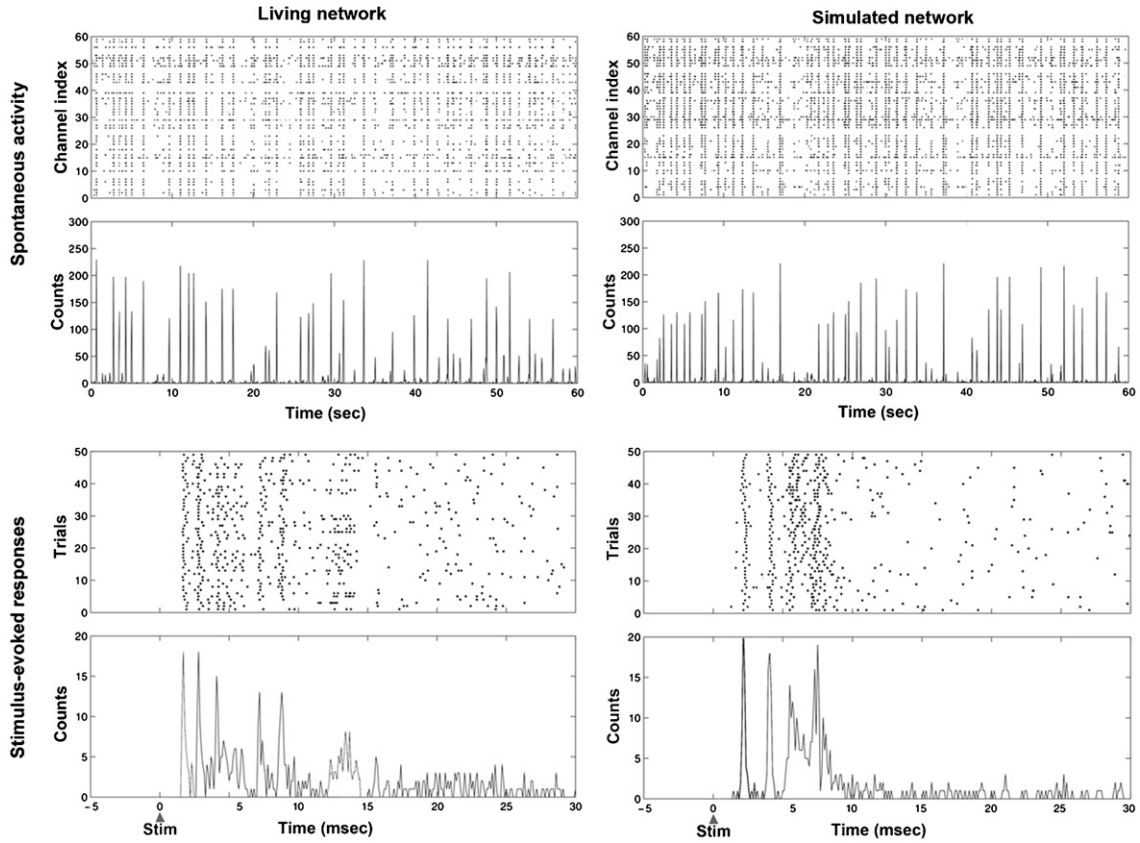

Figure 4. Comparison of the network activities from a MEA culture and a simulated network. Simulated spontaneous activity and evoked responses resemble the experimentally recorded data. First row: 1 min of spontaneous activity was recorded from a living network by a 60 channel MEA and in simulation for comparison. The upper panels are spike raster plots. The lower panels are firing rate histograms, with bin sizes of 100 ms. Second row: 50 trials of evoked responses recorded by one electrode in a living network and in simulation are shown for comparison. The upper panels are spike raster plots. The lower panels are firing rate histograms with a bin size of 0.1 ms. The timings of stimuli for each trial were aligned at time zero. In the simulation, each electrode recorded the activities occurring within 100 μm.

Table 1. Acronym list.

Abbreviation	Full name
Activity statistics	
FR	Firing rate
FRH	Firing rate histogram
MI	Mutual information
SCCC	Shift-predictor corrected cross-correlogram
CAT/CA	Center of activity trajectory/ center of activity
CAT-ELS	Center of activity trajectory with electrode locations shuffled
Analyses	
WIO vector	Whole-input–output vector
CW	Center of weights
MASC	Mean absolute synaptic change
C/D	Change-to-drift ratio
Others	
RPS	Random probing sequence
MEA	Multi-electrode array
LIF	Leaky-integrate-and-fire
STDP	Spike-timing-dependent Plasticity

several of these statistics in their ability to detect tetanus-induced network plasticity *in living cultures* on MEAs.

Network simulation: CAT showed the highest performance and sensitivity for detecting changes in the network synaptic state

In simulation, the synaptic connectivity can be easily controlled and monitored, and the way(s) changes in synaptic connectivity affect a statistic's value can be directly studied. Various statistics were used to study functional connectivity in simulated networks under different synaptic states. The performance of different activity statistics to small differences in network synaptic connectivity was evaluated by measuring the statistical significance of the change in each statistic under different network synaptic states, altered gradually by simulated tetanic stimulation with STDP.

Our 1000 neuron LIF model and the living networks expressed similar spontaneous, and evoked, activity patterns, demonstrating the ability of the LIF model to represent the activity of biological networks. Raster plots and FRH of spontaneous activity and evoked responses obtained from both MEA cultures and simulated networks are shown together for comparison, and demonstrate a remarkable similarity of activity patterns (figure 4) (Chao *et al* 2005). For example, the rates of barrages (the ongoing synchronized bursts of action potentials) were 0.70 Hz and 0.73 Hz, and the proportions of

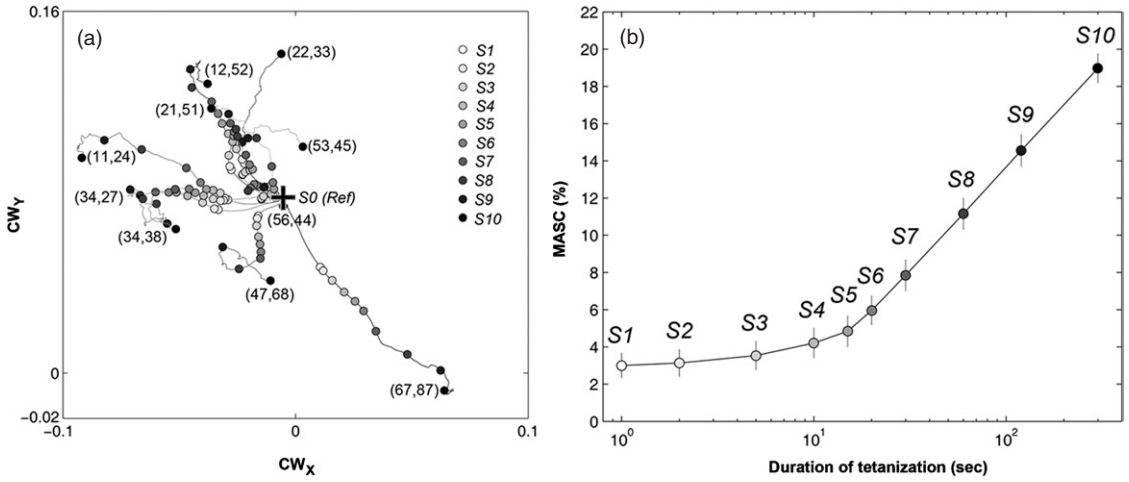

Figure 5. Setup of different synaptic states in simulation. A series of networks with different synaptic states were obtained by tetanization at different electrode pairs and with different durations from the reference network. From each reference network S_0, ten tetani at different electrode pairs were delivered. For each tetanization electrode pair, ten synaptic states were obtained after different durations. (a) Different tetanization electrode pairs caused different changes in synaptic weight distribution. The center of weights (CW) (see supplemental materials 7 available at stacks.iop.org/JNE/4/294) was used to visualize how the symmetry of the network synaptic weight distribution changed over time. Each curve represents CWs corresponding to a tetanization electrode pair (the column–row numbers of the electrodes are shown at the end of each curve). Synaptic states (S_1 to S_{10}) 'collected' at different tetanization durations and the corresponding reference state S_0 are shown as dots. (b) The relation between mean absolute synaptic change (MASC) and the duration of tetanization (note log scale) from five reference networks. The means and the standard deviations of MASCs are shown ($n = 50$ networks: from five reference networks, each with ten different tetani).

spikes in barrages were 76% and 71%, in spontaneous activity of living and simulated networks respectively.

A set of simulated networks with different synaptic states was created by using different electrode pairs and durations for tetanizations. In order to verify that different tetanization electrode pairs with different durations changed the synaptic weight distribution in the simulated networks, the centers of weights (CWs) (Chao *et al* (2005), see supplemental materials 7 available at stacks.iop.org/JNE/4/294) that were found for network states (S_0 to S_{10}) were calculated and are shown in figure 5(a).

CW represents the asymmetry of the network *synaptic weights* distribution. CW changed differently for different initial network synaptic weight distributions, for different tetanization electrode pairs and for different tetanization durations. Therefore, the various networks provide a basis to test the ability of various activity statistics to discriminate between synaptic states. The MASC of all different states (S_1 to S_{10}) relative to the initial S_0 is shown in figure 5(b). For each tetanization duration, the mean and standard deviation of MASC were calculated ($n = 50$ networks, from five reference networks and ten tetanization electrode pairs per reference network). Even with significantly different CWs, MASCs from different networks 'collected' at the same tetanization duration were similar in magnitude (standard deviation $<1\%$, $n = 50$), suggesting that the magnitude of plasticity was dependent mainly on tetanus duration, as opposed to the network structure.

Simulations with RPSs were performed on simulated networks with different synaptic weight distributions. The various activity statistics of evoked responses to the RPS were calculated from each simulation. An activity statistic with good discrimination of underlying synaptic states should show different results in different networks, even with only small differences in the distribution of synaptic weights.

CAT demonstrated the highest performance in detecting changes in state among the 6 statistics. The performances of the statistics are shown in figure 6. For each state S_i, the Euclidian distances $E(S_i)$ between each WIO vector of the statistic from S_i to the centroid of the WIO vectors from the corresponding S_0 were measured. Ten $E(S_i)$, measured from ten RPSs in the same network with the same tetanization electrode pair, were compared to ten corresponding $E(S_0)$, and the p-value was calculated ($n = 10$ RPSs, Wilcoxon signed rank test). For each state S_i, 50 p-values and 50 MASCs were collected from 50 networks (5 reference networks with 10 different tetanization electrode pairs per reference network). The mean and standard deviation of the p-values were plotted versus the corresponding MASC averaged across the networks ($n = 50$ networks). The detectable MASCs for CAT, JPSTH, SCCC, FRH, MI and FR were 4.68, 6.65, 6.75, 9.3, 11.7 and 15.7% respectively. CAT detected the smallest MASC and is therefore the best statistic.

The relative performance (the smaller the detectable MASC, the higher the performance), average compute time and dimensionality are shown in figure 7. The performance of the statistic shown in descending order is CAT, JPSTH, SCCC, FRH, MI and FR. The dimensionality of each statistic from one stimulation electrode is described in supplemental materials 2 (available at stacks.iop.org/JNE/4/294). The average compute times for CAT, FR, FRH, MI, SCCC and JPSTH were 31.8 s, 1.2 s, 30.6 s, 3.9 min, 26.4 min and 70.4 min per simulation respectively (MATLAB 7.0, AMD Athlon processor, 2.08 GHz, 512 MB RAM). Among all

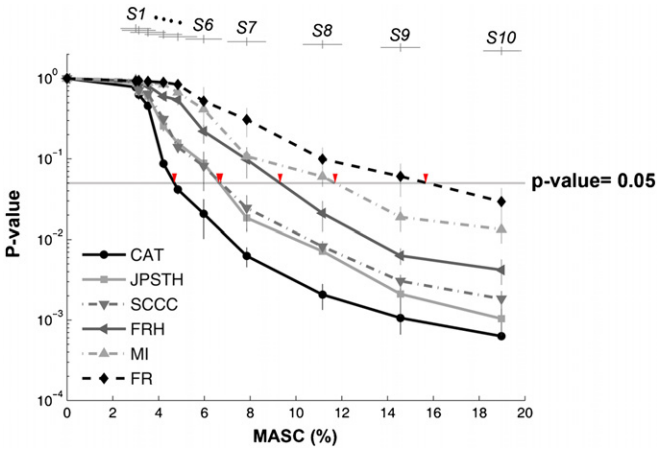

Figure 6. Evaluating the performances of different statistics. CAT showed the highest performance to detect changes in the synaptic state among six statistics. The performance of different statistics to detect changes in the synaptic state was evaluated by finding the 'detectable MASC' at the point the p-values reach a threshold of 0.05 (shown as arrows). For each state S_i, 50 p-values and 50 MASCs were collected from 50 networks (five reference networks with ten different tetanization electrode pairs per reference network, see results). The mean and standard deviation of the p-values ($n = 50$ networks) were plotted versus the corresponding MASC averaged across the networks ($n = 50$ networks). The mean and standard deviation of MASCs ($n = 50$ networks) are shown on the top of the figure (with vertical offsets for clarity). The performance of the statistic to detect the difference in MASC shown in descending order is CAT, JPSTH, SCCC, FRH, MI and FR.

six statistics, only FR and FRH had a shorter compute time than CAT, and only FR had smaller dimensionality than CAT. However, CAT showed significantly higher performance than FR and FRH.

Table 2 shows the occurrences of true positives, false negatives, false positives, true negatives and the sensitivity and specificity (see methods) of each statistic. CAT showed a sensitivity of 88.7%, the highest among all, with a specificity of 82.4%, comparable to JPSTH and SCCC. FRH, MI and FR showed high specificity, which was an artifact of their low sensitivities. Sixty-eight out of the 500 new network states were found to not have significantly different distributions of network synaptic weights as compared to their original reference states (two-sample Kolmogorov–Smirnov test, two-tailed, $\alpha = 0.05$).

By evaluating the performance, sensitivity, specificity and compute time, CAT was found to be most sensitive and highly efficient at detecting synaptic changes in simulated networks.

The five alternative statistics are often applied to spike-sorted data. Spike sorting is used to distinguish the spike trains of individual neurons (Ahissar *et al* 1998, Jimbo *et al* 1998, 1999, Celikel *et al* 2004), and can aid studies of neural populations (Lewicki 1998), especially for neural computations that use spike timing. In simulated networks, activity of individual neurons can be directly observed. The analysis in figure 6 was repeated using sorted neurons to investigate if the performance of the alternative statistics would improve. In the five reference simulated networks constructed, 4.1 ± 1.8 neurons were recorded per electrode, and the six statistics were recalculated based on about 250 neurons instead of 60 electrodes. CAT remained unchanged as the sorted spikes were spatially summed as before (see equation (1) in methods). Despite improved performance and sensitivity of the other five statistics, CAT *still* detected the most plasticity. JPSTH, SCCC, FRH, MI and FR improved 11.1, 17.6, 11.0, 35.0 and 31.2% in performance, respectively, and improved 1.9, 5.2, 9.7, 27.7 and 62.5% in sensitivity (see supplemental materials 4 available at stacks.iop.org/JNE/4/294).

Experiments in living cultures: CAT revealed tetanus-induced long-term plasticity significantly better than the other statistics

CAT was measured from the evoked responses to RPS in six experiments on living cultured cortical networks (CATs from all experiments are shown in supplemental materials 6 available at stacks.iop.org/JNE/4/294) and compared to the three most commonly used statistics: FR, FRH and SCCC. For visualization purposes, principal components analysis (PCA) was applied to the series of multi-dimensional WIO vectors to capture the largest variances and graphically demonstrate trends in changes. The first two principal components were normalized by subtracting their means and then dividing by their standard deviations. The normalized first principal component (PC1) was plotted versus the normalized second principal component (PC2). An example comparing CAT, FR, FRH and SCCC is shown in figure 8(a). The corresponding CATs before and after tetanization from every block (a 240 s window, see methods) and the average CATs are shown in figure 8(b).

The change across the tetanus was significantly greater than the drift before the tetanus for CAT ($p < 1 \times 10^{-4}$, Wilcoxon signed rank test), FRH ($p < 0.01$) and SCCC ($p < 0.01$), but not for FR ($p = 0.013$). C/D was used to quantify the change before the tetanus and the change across the tetanus (if the change is small, $C/D \cong 1$). The statistics of C/D from six experiments are shown in figure 8(c).

We did not perform spike sorting for experiments in living cultures. Standard spike sorting methods sort neural signals based on variations in spike waveform. In MEAs, local field potentials and overlapping action potentials distort the waveform to an extreme degree, and the electrodes are too far apart to allow triangulating common signal sources. Spike sorting was attempted, but proved to be unreliable.

Electrode shuffling demonstrates the importance of electrode locations shown by CAT

In order to get some idea of the degree of localization of function in cultured cortical networks, the performance of CAT statistic with electrode locations shuffled (CAT-ELS) was calculated (see supplemental materials 2 available at stacks.iop.org/JNE/4/294). In CAT-ELSs, the information about the physical locations of the recording electrodes was removed. In both simulations and experiments in living cultures, the electrode locations were shuffled ten times, and ten different corresponding CAT-ELSs were generated. The

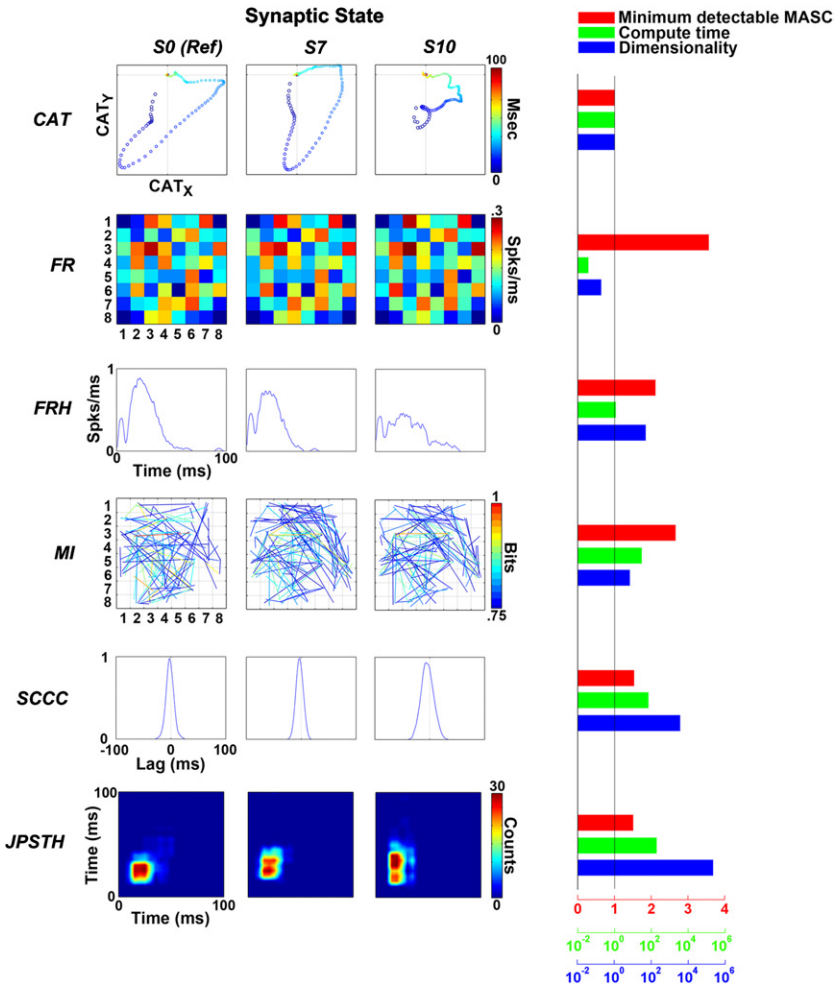

Figure 7. Comparison of the six different statistics. CAT was the most sensitive activity statistic and was highly efficient. Examples of six statistics calculated from the same RPS during three synaptic states are shown: S_0 (reference network), S_7 (network with ∼50% of the maximal MASC, see figure 5(b)) and S_{10} (network with the maximal MASC). All statistics were obtained from the same randomly chosen stimulation electrode. CAT: CATs are plotted as CAT_X versus CAT_Y from blue to red. FR: number of spikes per ms at each recording electrode is displayed according to the corresponding location in the 8 by 8 grids. FRH: FRHs, in the unit of number of spikes per ms, from a randomly chosen recording electrode are plotted. MI: MIs above 0.75 bits are plotted as colored lines between the corresponding electrode pairs. SCCC: SCCCs above zero from a randomly chosen pair of recording electrodes are plotted. JPSTH: JPSTH from the same randomly chosen pair of recording electrodes are shown. The performance (quantified by detectable MASC), compute time and dimensionality, normalized by the values for CAT, are shown on the right. The axes for detectable MASC, compute time and dimensionality are shown on the bottom in red, green and blue respectively (the latter two are with logarithmic scales). Among all six statistics, only FR and FRH had shorter compute time than CAT, and only FR had smaller dimensionality than CAT. However, CAT had significantly smaller detectable MASC than FR and FRH. CAT showed significantly higher performance to detect the difference in the network synaptic state than other statistics.

Table 2. Sensitivity versus specificity in simulated networks.

Statistic	CAT	JPSTH	SCCC	FRH	MI	FR	CAT-ELS (ten shuffles)
True positive (%)	77.6	70.4	68.0	47.4	44.0	27.2	30.6
False negative (%)	8.8	16.0	18.4	39.0	42.4	59.2	55.8
True negative (%)	11.2	11.0	11.2	12.2	13.6	13.6	12.6
False positive (%)	2.4	2.6	2.4	1.4	0	0	1.0
Sensitivity (%)	88.7	83.8	78.7	54.9	50.9	31.5	35.4
Specificity (%)	82.4	81.2	82.4	90.6	100	100	92.9

performance of these CAT-ELSs was evaluated and compared to the original CAT.

CAT, unlike the other statistics, incorporates the physical locations of the recording electrodes. This is the primary difference between methods, and we attribute CAT's superior performance in both living and simulated networks to this feature. For simulated networks, the comparison of the performance between CAT-ELS and original CAT is shown in figure 9(a). The detectable MASC (threshold p-value $= 0.05$) for mean CAT-ELS was 10.8%, which was worse than CAT

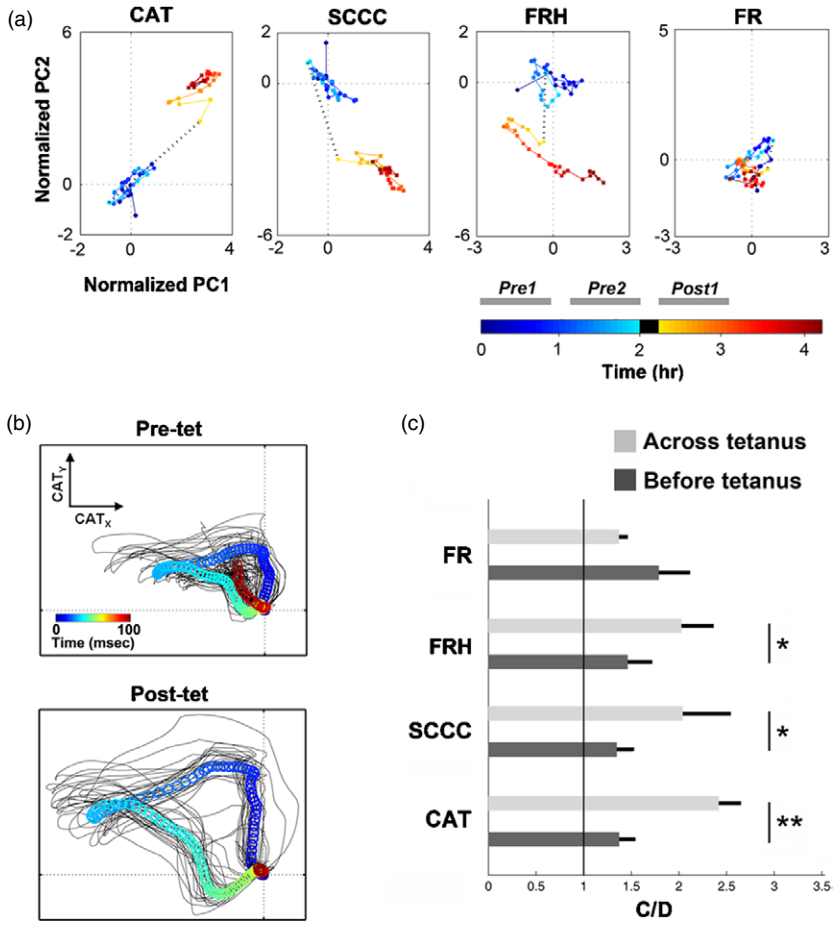

Figure 8. Comparison of the changes in CAT, FR, FRH and SCCC across tetanization in living MEA cultures. (a) An example of comparison of CAT, FR, FRH and SCCC (from evoked responses to RPS in one experiment) before and after tetanization is shown. Principal components analysis (PCA) was applied on multi-dimensional WIO vectors for visualization purposes. The normalized principal component was obtained by removing its mean and then dividing through by its standard deviation. The normalized first principal component (PC1) was plotted versus the normalized second principal component (PC2). Each dot represents the statistic calculated from every block (a 240 s window), and the color indicates the corresponding time (shown in the colorbar). The black dashed line represents the tetanus. The separation between pre-tetanization clusters (bluish dots) and post-tetanization clusters (reddish dots) indicates the change of the statistic across the tetanus. (b) Different patterns of CATs were observed before and after tetanization. CATs from an example experiment were overlaid (black trajectories), and the average CATs were shown by series of circles (from blue to red across 100 ms probe response). The trajectories for every experiment can be found in the supplemental materials 6 (available at stacks.iop.org/JNE/4/294). (c) The statistics of C/D from six experiments showed that the change across the tetanus was significantly greater than the drift before the tetanus for CAT (**, $p < 1 \times 10^{-4}$, Wilcoxon signed rank test), FRH (*, $p < 0.01$) and SCCC (*, $p < 0.01$), but not for FR ($p = 0.013$). The p-values indicate that CAT was more capable of detecting the change over the drift than FRH, SCCC and FR.

(4.68%). The decrease in performance (increase in detectable MASC) indicates that electrode locations significantly affect the performance of CAT in simulated networks. Furthermore, the sensitivity of CAT-ELS was 35.4%, significantly smaller than CAT's 88.7% (see table 2).

For living MEA cultures, one example of the comparison between CAT and CAT-ELS is shown in figure 9(b). The corresponding CAT-ELSs before and after tetanization from every block are shown in figure 9(c). The electrode location shuffling 'collapsed' the patterns of CAT-ELSs before and after tetanization (compare to figure 8(b)). The difference between pre-tetanization and post-tetanization clusters found in CAT was also reduced in CAT-ELS (figure 9(b)).

The statistics of C/D for CAT-ELS ($n = 60$, six experiments, ten shuffles for each experiment) are shown in figure 9(d). The change across the tetanus was significantly greater than the drift before the tetanus for CAT ($p < 1 \times 10^{-4}$, Wilcoxon signed rank test), but not for CAT-ELS ($p = 0.19$).

Discussion

Statistics of functional plasticity in extracellular multi-electrode recordings

While comparisons of firing rates show plasticity in intracellular recordings, more detailed statistics incorporating spatiotemporal population activity patterns are needed to reveal plasticity in extracellular multi-electrode recordings. Electrode spacing on the order of hundreds of microns means that any induced or observed plasticity will span pathways of multiple neurons instead of neighboring monosynaptic neurons (Jimbo *et al* 1999). Intracellularly, synaptic strength

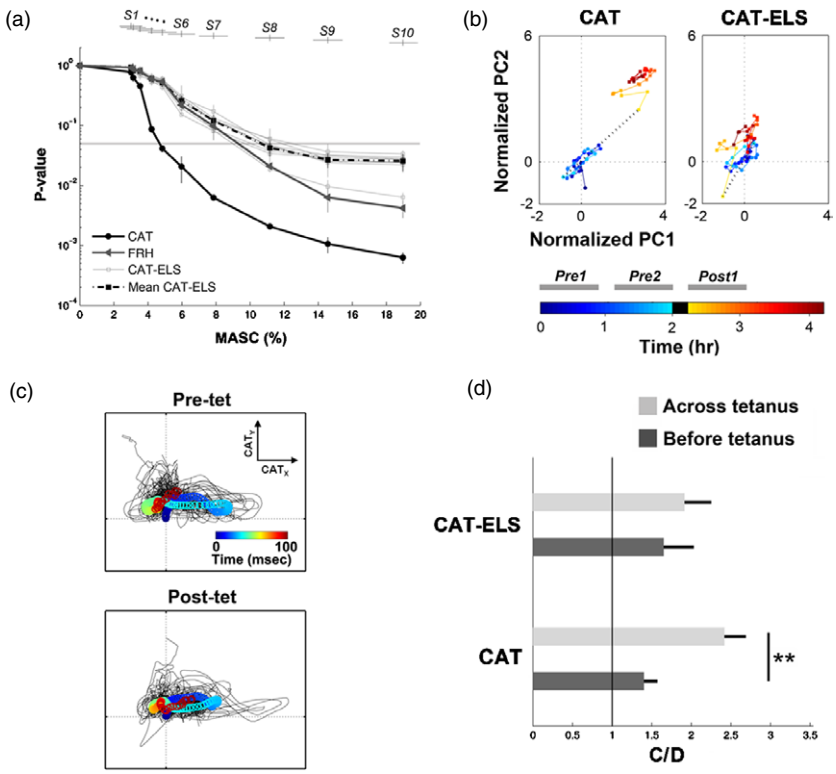

Figure 9. Comparison of CAT and CAT-ELS in simulated and living networks. (a) A comparison of the performance of CAT and CAT-ELS in simulated networks (the representation is the same as figure 6). Ten performance curves corresponding to different random shuffled electrode locations (CAT-ELS) and the mean of the ten curves (Mean CAT-ELS) are shown. The performance curve of FRH is also shown for comparison. The detectable MASC (threshold p-value $= 0.05$) for mean CAT-ELS was 10.8%, which was greater than CAT (4.68%). The decrease in performance (increase in detectable MASC) indicates the importance of physical electrode locations in the performance of CAT in simulated networks. (b) An example comparison of CAT and CAT-ELS in a living MEA culture before and after tetanization (the data used and representation are the same as in figure 8(a)). The difference between pre-tetanization clusters (bluish dots) and post-tetanization clusters (reddish dots) was reduced by shuffling electrode locations in CAT-ELS. (c) The electrode locations shuffling 'collapsed' the patterns of CAT-ELSs before and after tetanization in a living MEA culture. The difference between before and after tetanization trajectories (compared to figure 8(b)) was reduced in CAT-ELS. (d) The statistics of C/D for CAT-ELS in living networks ($n = 60$, six experiments, ten shuffles for each experiment). The change across the tetanus was not significantly different than the drift before the tetanus ($p = 0.19$, Wilcoxon signed rank test), unlike CAT (**, $p < 1 \times 10^{-4}$). Thus, for both simulated and living networks, the shuffling of signals from different electrodes greatly reduces the performance of CAT for detecting stimulus-induced synaptic change over a background of continual synaptic drift.

is directly observable by stimulating a pre-synaptic neuron while recording from an adjacent post-synaptic neuron. Extracellularly, synaptic noise across a chain of neurons and convergent pathways will obscure firing rate measures of stimulus-induced plasticity.

Alternatively, by incorporating the timing and spatial flow of activity, spatiotemporal patterns have been found both *in vivo* and *in vitro*. Spike sequences, imposed upon the network by behavioral manipulations, recur spontaneously during subsequent sleep episodes (Nádasdy *et al* 1999, Nádasdy 2000, Lee and Wilson 2002). Calcium imaging of cortical slices reveals reactivation of sequences of neurons, 'cortical songs', with distinct spatiotemporal structures over tens of seconds (Ikegaya *et al* 2004). Robust recurrent spike patterns were also found in a detailed cortical simulation (Izhikevich *et al* 2004) and in living slices (Fellous *et al* 2004). CAT provides a new and simple statistic to detect spatiotemporal patterns in networks and extends the previous studies by quantifiably demonstrating its ability to discern plasticity.

Region-specific plasticity

Although FRH included detailed temporal information about the activity dynamics at all electrodes, it was less capable of capturing network plasticity than CAT, which has the same temporal resolution as the FRH but 'condenses' the spatial dimension by linear combination (see equation (1)). We hypothesize that this was due to the inclusion of spatial information of the electrode locations. The performance and the sensitivity of CAT with electrode locations shuffled were significantly worse than unshuffled CAT, both in simulation (the detectable MASC increased from 4.68% to 10.8% and the sensitivity decreased from 88.7% to 35.4%) and in living networks (the change across the tetanus was significantly greater than the drift before the tetanus for CAT, but not for CAT-ELS) (see figure 9 and table 2). This indicates that activity varied systematically with the electrode location, and also suggested that the observed network plasticity was *region specific*: the plasticity was not symmetrically distributed throughout the network. This further suggests that despite

the apparent random connectivity of cultured neurons, neuron location played a role in tetanus-induced plasticity.

Region specificity was not limited to plasticity induced by tetanization. In simulation, we also altered the weights of randomly selected synapses in reference networks to different degrees to generate different new network states. CAT still showed the highest sensitivity to changes in MASC, and furthermore, the sensitivity of CAT-ELS was still significantly lower (data not shown). Despite the synaptic plasticity not being region specific, the spatiotemporal flow of neural activity was region dependent, effectively making the plasticity of neural activity region specific. This result supports the notion of synfire chains or braids of neural activity (Ikegaya *et al* 2004, Izhikevich 2005), where information is transmitted in a pipeline of neighboring pathways as opposed to a single string of connections. In this study, tetanization was used to obtain different synaptic states since it provided a realistic form of plasticity and a straightforward comparison to our study of local functional plasticity in living networks.

A common misconception regarding dissociated cultures is that they are random, homogeneous and lack structure, and thus cannot support stable changes to synaptic weights associated with memory formation. While plated from a random cell suspension, microscopic observation reveals that a heterogeneous arrangement develops over time (Gross and Kowalski 1999, Segev *et al* 2003). Although very different than structures found *in vivo*, the ability of neurons and glia to interact remains and a network having a diverse array of activity arises spontaneously (Wagenaar *et al* 2006b). Altering sensory input of thalamic relays to cortical areas has demonstrated that the cortex develops structure according to the type of the sensory input (Sur *et al* 1988), which suggests an important relationship between neural structure and function. CAT demonstrates that structure is also relevant to neural function in a cultured network, and that tetanic stimulation alters network function. Future experiments will incorporate closed-loop sensory-motor feedback and optical imaging to investigate the network mechanisms of our cultures to functionally and structurally adapt to environmental interaction (Potter *et al* 2006).

CAT versus population coding

It is important to note that CAT is distinct from the population vector description of neural activity (Georgopoulos *et al* 1986, Caminiti *et al* 1990). Population coding, which is widespread in the brain and in invertebrate nervous systems, has been found in the motor cortex (Georgopoulos 1994), premotor cortex (Caminiti *et al* 1990), hippocampus (Wilson and McNaughton 1993) and other cortical areas. It demonstrates how the firing rates of a group of broadly tuned (e.g., to a direction of arm movement) neurons, taken together, provide an accurately tuned representation. With population codes, a fixed-weight linear combination of neuronal activity is projected in a sensory input space or a motor output space (Carmena *et al* 2003). In contrast, CAT incorporates information about the physical recording locations into its linear combination calculation, and projects neuronal activities recorded at different sites into the actual neuronal location space in order to depict the dynamics of the population activity. Furthermore, the linear combination of activities in CAT is normalized by the total firing rate across all electrodes (see equation (1)).

CA is a measure of the asymmetry of the spatial activity distribution, and CAT is a measure of its dynamics. A similar measure of population activity flow was applied in human study to quantify the trajectory patterns of the traveling electroencephalographic alpha waves across the scalp (Manjarrez *et al* 2007).

Plasticity versus spontaneous bursting

Without external stimulation, the most prominent feature of spontaneous activity found in MEA cultures and in simulated networks is synchronous bursting (Wong *et al* 1993, Kamioka *et al* 1996, Gross and Kowalski 1999, Van Pelt *et al* 2004, Wagenaar *et al* 2005), and bursts were found to have effects on tetanus-induced synaptic plasticity in cortical neurons (Maeda *et al* 1998). In simulation, the network synaptic state after tetanization was found to change gradually due to the presence of spontaneous bursts, which makes quantifying tetanus-induced plasticity difficult (Chao *et al* 2005). In the six experiments we performed on living MEA cultures, 8.57 ± 3.33 spontaneous bursts per minute and 16.06 ± 4.55 stimulus-evoked bursts per minute were observed. Even with the presence of the spontaneous bursts, the tetanus-induced plasticity was still detected by using CAT. Since the level of bursting can be finely controlled in MEA cultures with multi-site stimulation (Wagenaar *et al* 2005), we plan to use CAT to investigate how the degree of bursting affects a network's ability to produce and/or maintain plasticity.

CAT's superior performance, sensitivity and low computational load make it an attractive method for real-time applications. CAT can also be applied to *in vivo* multi-electrode or optical recording studies for neural activity aligned to behavioral or sensory cues. As techniques for observing distributed activity become faster and more fine-grained, studying the details of the spatial flow of activity through neuronal networks will reveal more and more about processes of learning and memory.

Acknowledgments

This work was partially supported by grants NS38628 from NIH/NINDS, EB000786 from NIH/NIBIB and DA18250 from NIH/NIDA, and by the Whitaker Foundation and the NSF Center for Behavioral Neuroscience. We thank Radhika Madhavan for technical assistance and Douglas Swehla for valuable inputs.

References

Ahissar E, Abeles M, Ahissar M, Haidarliu S and Vaadia E 1998 Hebbian-like functional plasticity in the auditory cortex of the behaving monkey *Neuropharmacology* **37** 633–55

Ahissar E, Vaadia E, Ahissar M, Bergman H, Arieli A and Abeles M 1992 Dependence of cortical plasticity on correlated activity of single neurons and on behavioral context *Science* **257** 1412–5

Bao S, Chang E F, Davis J D, Gobeske K T and Merzenich M M 2003 Progressive degradation and subsequent refinement of acoustic representations in the adult auditory cortex *J. Neurosci.* **23** 10765–75

Baruchi I and Ben-Jacob E 2004 Functional holography of recorded neuronal networks activity *J. Neuroinform.* **2** 333–52

Bi G Q and Poo M M 1998 Synaptic modifications in cultured hippocampal neurons: dependence on spike timing, synaptic strength, and postsynaptic cell type *J. Neurosci.* **18** 10464–72

Bliss T V and Lømo T 1973 Long-lasting potentiation of synaptic transmission in the dentate area of the anaesthetized rabbit following stimulation of the perforant path *J. Physiol.* **232** 331–56

Brown E N, Kass R E and Mitra P P 2004 Multiple neural spike train data analysis: state-of-the-art and future challenges *Nat. Neurosci.* **7** 456–61

Buonomano D V 1998 Cortical plasticity: from synapses to maps *Ann. Rev. Neurosci.* **21** 149–86

Caminiti R, Johnson P B, Burnod Y, Galli C and Ferraina S 1990 Shifts of preferred directions of premotor cortical cells with arm movements performed across the workspace *Exp. Brain Res.* **83** 228–32

Carmena J M, Lebedev M A, Crist R E, O'Doherty J E, Santucci D M, Dimitrov D F, Patil P G, Henriquez C S and Nicolelis M A L 2003 Learning to control a brain–machine interface for reaching and grasping by primates *PLoS Biol.* **1** 1–16

Celikel T, Szostak V A and Feldman D E 2004 Modulation of spike timing by sensory deprivation during induction of cortical map plasticity *Nat. Neurosci.* **7** 534–41

Chao Z C, Bakkum D J, Wagenaar D A and Potter S M 2005 Effects of random external background stimulation on network synaptic stability after tetanization—a modeling study *Neuroinformatics* **3** 263–80

Chornoboy E S, Schramm L P and Karr A F 1988 Maximum likelihood identification of neural point process systems *Biol. Cybern.* **59** 265–75

David O, Cosmelli D and Friston K J 2004 Evaluation of different measures of functional connectivity using a neural mass model *Neuroimage* **21** 659–73

Delaney K R, Zucker R S and Tank D W 1989 Calcium in motor nerve terminals associated with posttetanic potentiation *J. Neurosci.* **9** 3558–67

Fellous J-M, Tiesinga P H E, Thomas P J and Sejnowski T J 2004 Discovering spike patterns in neuronal responses *J. Neurosci.* **24** 2989–3001

Fisher S A, Fischer T M and Carew T J 1997 Multiple overlapping processes underlying short-term synaptic enhancement *Trends Neurosci.* **20** 170–7

Fortune E S and Rose G J 2000 Short-term synaptic plasticity contributes to the temporal filtering of electrosensory information *J. Neurosci.* **20** 7122

Georgopoulos A, Schwartz A and Kettner R 1986 Neuronal population coding of movement direction *Science* **233** 1416–9

Georgopoulos A P 1994 Population activity in the control of movement *Selectionism and the Brain* (San Diego: Academic) pp 103–19

Gerstner W, Kempter R, van Hemmen J L and Wagner H 1996 A neuronal learning rule for sub-millisecond temporal coding *Nature* **6595** 76–7

Gross G W 1979 Simultaneous single unit recording in vitro with a photoetched laser deinsulated gold multimicroelectrode surface *IEEE Trans. Biomed. Eng.* **26** 273–9

Gross G W and Kowalski J M 1999 Origins of activity patterns in self-organizing neuronal networks in vitro *J. Intell. Mater. Syst. Struct.* **10** 558–64

Ikegaya Y, Aaron G, Cossart R, Aronov D, Lampl I, Ferster D and Yuste R 2004 Synfire chains and cortical songs: temporal modules of cortical activity *Science* **304** 559–64

Izhikevich E M 2005 Polychronization: computation with spikes *Neural Comput.* **18** 245–82

Izhikevich E M, Gally J A and Edelman G M 2004 Spike-timing dynamics of neuronal groups *Cereb. Cortex* **14** 933–44

Jimbo Y, Robinson H P C and Kawana A 1998 Strengthening of synchronized activity by tetanic stimulation in cortical cultures: application of planar electrode arrays *IEEE Trans. Biomed. Eng.* **45** 1297–304

Jimbo Y, Tateno T and Robinson H P C 1999 Simultaneous induction of pathway-specific potentiation and depression in networks of cortical neurons *Biophys. J.* **76** 670–8

Kamioka H, Maeda E, Jimbo Y, Robinson H P C and Kawana A 1996 Spontaneous periodic synchronized bursting during formation of mature patterns of connections in cortical cultures *Neurosci. Lett.* **206** 109–12

Kudrimoti H S, Barnes C A and McNaughton B L 1999 Reactivation of hippocampal cell assemblies: effects of behavioral state, experience, and EEG dynamics *J. Neurosci.* **19** 4090–101

Leahy R M, Mosher J C, Spencer M E, Huang M X and Lewine J D 1998 A study of dipole localization accuracy for MEG and EEG using a human skull phantom *Electroencephalogr. Clin. Neurophysiol.* **107** 159–73

Lee A and Wilson M 2002 Memory of sequential experience in the hippocampus during slow wave sleep *Neuron* **36** 1183–94

Levy W B and Steward O 1983 Temporal contiguity requirements for long-term associative potentiation/depression in the hippocampus *Neuroscience* **8** 791–7

Lewicki M S 1998 A review of methods for spike sorting: the detection and classification of neural action potentials *Network* **9** R53–78

Maeda E, Kuroda Y, Robinson H P C and Kawana A 1998 Modification of parallel activity elicited by propagating bursts in developing networks of rat cortical neurons *Eur. J. Neurosci.* **10** 488–96

Manjarrez E, Vazquez M and Flores A 2007 Computing the center of mass for traveling alpha waves in the human brain *Brain Res.* **1145** 239–47

Markram H, Gupta A, Uziel A, Wang Y and Tsodyks M 1998 Information processing with frequency-dependent synaptic connections *Neurobiol. Learn. Mem.* **70** 101–12

Merzenich M and Sameshima K 1993 Cortical plasticity and memory *Curr. Opin. Neurobiol.* **3** 187–96

Miles R and Wong R K 1987 Inhibitory control of local excitatory circuits in the guinea-pig hippocampus *J. Physiol.* **388** 611–29

Morris K F, Baekey D M, Nuding S C, Dick T E, Shannon R and Lindsey B G 2003 Invited review: neural network plasticity in respiratory control *J. Appl. Physiol.* **94** 1242–52

Nádasdy Z 2000 Spike sequences and their consequences *J. Physiol.* **94** 505–24

Nádasdy Z, Hirase H, Czurkó A, Csicsvari J and Buzsáki G 1999 Replay and time compression of recurring spike sequences in the hippocampus *J. Neurosci.* **19** 9497–507

Natschläger T, Markram H and Maass W 2002 Computer models and analysis tools for neural microcircuits *Neuroscience Databases. A Practical Guide* ed R Kötter (Boston, MA: Kluwer Academic) pp 123–38

Okatan M, Wilson M A and Brown E N 2005 *Analyzing Functional Connectivity Using a Network Likelihood Model of Ensemble Neural Spiking Activity* (Cambridge, MA: MIT Press)

Pine J 1980 Recording action potentials from cultured neurons with extracellular microcircuit electrodes *J. Neurosci. Methods* **2** 19–31

Potter S M and DeMarse T B 2001 A new approach to neural cell culture for long-term studies *J. Neurosci. Methods* **110** 17–24

Potter S M, Wagenaar D A and DeMarse T B 2006 Closing the loop: stimulation feedback systems for embodied MEA cultures *Advances In Network Electrophysiology Using Multi-Electrode Arrays* ed M Taketani and M Baudry (Dordrecht: Kluwer, Springer)

Reich D S, Victor J D, Knight B W, Ozaki T and Kaplan E 1997 Response variability and timing precision of neuronal spike trains in vivo *J. Neurophysiol.* **77** 2836–41

Rosenkranz J A and Grace A A 1999 Modulation of basolateral amygdala neuronal firing and afferent drive by dopamine receptor activation in vivo *J. Neurosci.* **19** 11027

Ruaro M E, Bonifazi P and Torre V 2005 Toward the neurocomputer: image processing and pattern recognition with neuronal cultures *IEEE Trans. Biomed. Eng.* **52** 371–83

Scherg M 1990 Fundamentals of dipole source potential analysis *Adv. Audiol.* **6** 40–69

Segev R, Benveniste M, Shapira Y and Ben-Jacob E 2003 Formation of electrically active clusterized neural networks *Phys. Rev. Lett.* **90** 168101

Shefi O, Golding I, Segev R, Ben-Jacob E and Ayali A 2002 Morphological characterization of in vitro neuronal networks *Phys. Rev.* E **66** 021905

Song S, Miller K D and Abbott L F 2000 Competitive Hebbian learning through spike-timing-dependent synaptic plasticity *Nat. Neurosci.* **3** 919–26

Sur M, Garraghty P and Roe A 1988 Experimentally induced visual projections into auditory thalamus and cortex *Science* **242** 1437–41

Van Pelt J, Wolters P S, Corner M A, Rutten W L C and Ramakers G J A 2004 Longterm characterization of firing dynamics of spontaneous bursts in cultured neural networks *IEEE Trans. Biomed. Eng.* **51** 2051–62

Wagenaar D, Madhavan R, Pine J and Potter S 2005 Controlling bursting in cortical cultures with closed-loop multi-electrode stimulation *J. Neurosci.* **25** 680–8

Wagenaar D, Pine J and Potter S 2004 Effective parameters for stimulation of dissociated cultures using multi-electrode arrays *J. Neurosci. Methods* **138** 27–37

Wagenaar D, Pine J and Potter S M 2006a Searching for plasticity in dissociated cortical cultures on multi-electrode arrays *J. Negat. Results Biomed.* **5** 16

Wagenaar D A, Pine J and Potter S M 2006b An extremely rich repertoire of bursting patterns during the development of cortical cultures *BMC Neurosci.* **7** 11

Wagenaar D A and Potter S M 2002 Real-time multi-channel stimulus artifact suppression by local curve fitting *J. Neurosci. Methods* **120** 113–20

Wagenaar D A and Potter S M 2004 A versatile all-channel stimulator for electrode arrays, with real-time control *J. Neural Eng.* **1** 39–44

Wilson M and McNaughton B 1993 Dynamics of the hippocampal ensemble code for space *Science* **261** 1055–8

Wojtowicz J M and Atwood H L 1985 Correlation of presynaptic and postsynaptic events during establishment of long-term facilitation at crayfish neuromuscular junction *J. Neurophysiol.* **54** 220–30

Wong R O L, Meister M and Shatz C J 1993 Transient period of correlated bursting activity during development of the mammalian retina *Neuron* **11** 923–38

Supplement for:

Region-specific Network Plasticity in Simulated and Living Cortical Networks: Comparison of the Center of Activity Trajectory (CAT) With Other Statistics

Zenas C. Chao, Douglas J. Bakkum and Steve M. Potter

S1: Simulated networks.

Features:

The Neural Circuit SIMulator (Natschlager et al., 2002) was used to produce five artificial neural networks as described previously (Chao et al., 2005). Briefly, 1,000 leaky-integrate-and-fire (LIF) model neurons with a total of 50,000 synapses were placed randomly in a 3mm by 3mm area (see figure 1(c)). All synapses were frequency-dependent (Markram et al., 1998; Izhikevich et al., 2004) to model synaptic depression. 70% of the neurons were excitatory, with spike-timing dependent plasticity (STDP) (Song et al., 2000). The other neurons were inhibitory (30%) (Marom and Shahaf, 2002). Neurons made many short synaptic connections but a few long ones as well (Segev and Ben-Jacob, 2000). The number of synaptic connections per neuron followed a Gaussian distribution and each neuron had 50 ± 33 synapses onto other neurons (no multiple synapses from one neuron to another). The conduction delay was proportional to the distance between somata, and the conduction velocity was set to be 0.3 m/s (Kawaguchi and Fukunishi, 1998). Gaussian random noise was introduced into each neuron independently as fluctuations in membrane voltage: 30% of the neurons ("self-firing neurons") had variance at a high enough level to initiate spikes (Latham et al., 2000), while the

rest exhibited only subthreshold fluctuations. An 8 by 8 grid of electrodes was included, 60 of these (except corner electrodes 11, 18, 81 and 88) were used for recording and stimulation as in a real MEA (figure 1(d)). A stimulation electrode stimulated 76 ± 12 (n= 5 simulated networks) of the closest model neurons.

Setup of network initial states:

All excitatory synaptic weights were initially set to 0.25 and could vary between zero and 0.5 due to STDP. At the maximal weight, each spike would have a 90% probability of evoking a spike in the post-synaptic neuron, due to its summation with intrinsic noise. The synaptic weights for the inhibitory connections were fixed at -0.25. The networks were run for 5 hours in simulated time until the synaptic weights reached a steady state. Most of the excitatory synaptic weights (92 ± 3%) in the 5 reference networks were less than 0.05 or greater than 0.45. This bimodal steady-state distribution of weights arose from the STDP rule, as previously observed by Song et al.(Song et al., 2000), and Izhikevich and Desai (Izhikevich and Desai, 2003). The set of synaptic weights after 5 hours of spontaneous activity stabilized, without external stimuli, and was used as the initial state for the corresponding reference network.

S2: Calculations of the statistics for experiments in simulations and living cultures.

The evoked responses within 100 msec (to include all evoked responses) after the stimuli of random probing sequences (RPSs) were used for calculations of the statistics. The dimensionalities of different statistics are shown in Table S1. For those statistics include temporal information (FRH, MI, SCCC, JPSTH, and CAT), responses within 100 msec were binned by a 5 msec moving time bin with 500 μsec time step. 500 μsec time step was used to obtain fine temporal resolution, since it was less than the occurrence of an action potential. 5 msec bin size was used to acquire action potentials on multiple electrodes within a single bin. Also, the same binning parameters were used for all statistics in simulations and in living cultures for fair comparison of their performance.

1. Simulations:

Firing Rate (FR)

This most commonly used statistic quantifies the intensity of the evoked responses. During each simulation, stimuli at each electrode occurred multiple times (10.0 ± 3.1 trials) in one RPS. FR for evoked responses to each stimulation electrode was calculated by averaging the number of spikes counted at each recording electrode over trials, producing a 60-dimensional vector.

Firing Rate Histogram (FRH)

FRH expands on FR by including temporal information. FRH from recording electrode E_k to the probing stimulus at electrode P_i, $FRH_{E_k}^{P_i}$, was the average number of spikes counted in a 5 msec moving time window with 500 μsec time

step over trials, which resulted in a 1X191 vector. FRH for evoked responses to stimulation electrode P_i was defined by joining $FRH_{E_k}^{P_i}$ from 60 recording electrodes together, which formed an 11,460-dimensional (191X60) vector.

Center of Activity Trajectory (CAT)

The definition of CAT is described in Methods (Equation 1 and 2). The X and Y components are both 1X191 vectors. By appending two components together, CAT for evoked responses to each stimulation electrode was a 382-dimensional (191X2) vector.

Mutual Information (MI)

MI quantifies the statistical dependence, including higher order moments in addition to 2nd order, between responses at different locations (Moddemeijer, 1989; Brunel and Nadal, 1998; Paninski, 2003). MI between two recording electrodes E_k and E_j for stimulation electrode P_i is defined as the mutual information between two distributions: $FRH_{E_k}^{P_i}$ and $FRH_{E_j}^{P_i}$. Let $FRH_{E_k}^{P_i} = \{A_n\}_{n=1}^{191}$ and $FRH_{E_j}^{P_i} = \{B_m\}_{m=1}^{191}$, where A_n and B_m represent elements in *FRH*s. Then the MI between $FRH_{E_k}^{P_i}$ and $FRH_{E_j}^{P_i}$ is defined as:

$$I(FRH_{E_k}^{P_i}, FRH_{E_j}^{P_i}) = \sum_{n,m} P_{X,Y}(A_n \times B_m) \ln \frac{P_{X,Y}(A_n \times B_m)}{P_X(A_n) \times P_Y(B_m)}$$

where P_X and P_Y represent the marginal probabilities of $FRH_{E_k}^{P_i}$ and $FRH_{E_j}^{P_i}$, and $P_{X,Y}$ represents the joint probability of $FRH_{E_k}^{P_i}$ and $FRH_{E_j}^{P_i}$. MI was estimated by using the histogram-based mutual information methods described by Moddemeijer (Moddemeijer, 1989). In this study, the MATLAB codes from

Rudy Moddemeijer's group were used[1]. MI provides a non-directional connectivity map, which represents the dependence between activities at different pairs of electrodes. By joining the MI from every pair of electrodes, MI for evoked responses to each stimulation electrode was a 1,770-dimensional (60X59/2) vector.

Shift-predictor Corrected Cross-Correlogram (SCCC)

The corrected cross-correlogram (Michalski et al., 1983; Eggermont, 1992; Brody, 1999; Franco et al., 2004; Ventura et al., 2005) removes the peak in the original cross-correlogram that is due to co-stimulation of the neurons, and measures the association between neurons. For each pair of recording electrodes, the "raw" cross-correlogram was constructed by averaging the cross-correlograms between two spike trains from the two electrodes over trials. The "shift predictor" was constructed by averaging the cross-correlograms between all possible pairs of spike trains from the two electrodes but from different trials. SCCC was then the raw cross-correlogram minus the shift predictor. In this study, the algorithm described by George Gerstein's group was used[2].

With the same binning resolution used for FRH, SCCC between each pair of recording electrodes was a (191X2-1)-dimensional vector which represents the correlations sequence at different lags. Therefore, SCCC for evoked responses to each stimulation electrode was a 674,370-dimensional ((191X2-1)X60X59/2) vector.

[1] http://www.cs.rug.nl/~rudy/papers/abstracts/RM8902.html
[2] http://mulab.physiol.upenn.edu/crosscorrelation.html

Joint Peri-Stimulus Time Histogram (JPSTH)

The JPSTH quantifies the causality between responses at different locations (Gerstein and Perkel, 1969; Aertsen et al., 1989; Ventura et al., 2005). JPSTH finds the fixed delay between sequences of spikes recorded at different pairs of neurons (electrodes) over multiple trials, which can depict causal relationships between them. Similar to SCCC, the shift-predictor was applied on the "raw" JPSTH to eliminate the time-locked stimulus-induced covariation due to co-stimulation. In this study, the algorithm and MATLAB codes from George Gerstein's group were used[3]. The results can provide directional information about the connectivity. With the same binning resolution used for FRH, JPSTH between each pair of recording electrodes was 191X191-dimensional. Therefore, JPSTH for evoked responses to each stimulation electrode was a 64,571,370-dimensional (191X191X60X59/2) vector.

Center of Activity Trajectory with Electrode Locations Shuffled (CAT-ELS)

The electrode locations, E_k, were randomly shuffled. Then CAT-ELS was calculated according to Equation 1 and 2 (in Methods) by using these shuffled electrode locations. For each network, the electrode locations were shuffled 10 times and 10 different corresponding CAT-ELSs were generated.

2. Experiments in living cultures:

Firing Rate (FR)

The number of spikes was counted at each recording electrode for each probe response and averaged every block. Thus, for each stimulation electrode, a

[3] http://mulab.physiol.upenn.edu/jpst.html

60-dimensional FR vector was obtained for every 240 sec ("block", see Methods).

Firing Rate Histogram (FRH)

For evoked responses to each stimulus, the FRH was calculated by using a 5 msec moving time window with time step of 500 μsec. Thus, for each stimulation electrode, an 11,460-dimensional (191X60) FRH vector was obtained for every block.

Center of Activity Trajectory (CAT)

Let $FRH_{E_k}^{P_i}$ be the average responses over each block, recorded at electrode E_i to stimulation electrode P_i. CAT for stimulation electrode P_i was then calculated from the $FRH_{E_k}^{P_i}$ by using Equation 1 and 2 (in Methods). Thus, for each stimulation electrode, a 382-dimensional (191X2) CAT vector was obtained for every block.

Shift-predictor Corrected Cross-Correlogram (SCCC)

With the same binning resolution used for FRH, SCCC between each pair of recording electrodes was calculated for every block. Thus, for each stimulation electrode, a 674,370-dimensional ((191X2-1)X60X59/2) SCCC vector was obtained for every block.

Center of Activity Trajectory with Electrode Locations Shuffled (CAT-ELS)

CAT-ELS was calculated by the same shuffling procedure used in simulations. For each experiment, the electrode locations were shuffled 10 times and 10

different corresponding CAT-ELSs were generated. The dimensionality of CAT-ELS was the same as CAT.

Table S1. The dimensionality of the statistics.

Statistics	Dimensionality[1]	
	Simulations	Experiments in living cultures
FR	60	60
FRH	11,460	11,460
MI	1,770	-
CAT	382	382
CAT_ELS	382	382
SCCC	674,370	674,370
JPSTH	64,571,370	-

[1] The dimensionality is defined as the length of the statistic calculated from evoked responses to *one* stimulation electrode in one simulation or in one block (for experiments in living cultures).

S3: Movie of CATs in a simulated network.

Different patterns of CATs were obtained from evoked responses to stimuli at different electrodes in simulation (see **Movie S3**). **A.** The rasterplot of 1 second of network activity from 1000 LIF neurons. Evoked responses to stimuli at different electrodes are shown in different colors. **B.** 1000 neurons on 3mm by 3mm area. Neurons are shown as gray dots, and the active synapses are shown in cyan lines. The locations of stimulation electrodes are indicated by crosses with the corresponding colors shown in A. **C.** The corresponding CATs. The color of the trajectory represents the corresponding evoked response shown in A. Time is represented in the red bar at the bottom of A.

S4: Performances of the 6 statistics after spike sorting in simulated networks.

Sorting recorded action potentials and recalculating the activity statistics improved the performance of all except for CAT. However, the CAT still showed the highest performance. The calculation of the CAT remained the same as the sorted spikes are spatially summed according to recording electrode locations The six statistics were re-calculated based on the activity of about 250 spike sorted neurons instead of 60 electrodes (see Results).JPSTH, SCCC, FRH, MI and FR improved 11.1, 17.6, 11.0, 35.0 and 31.2 %, respectively. The same figure representation was used as in Figure 7. The sensitivities and specificities for these statistics (also see Discussion) are shown in the table.

Statistic	*CAT*	*JPSTH*	*SCCC*	*FRH*	*MI*	*FR*
Sensitivity (%)	88.7	85.4	82.8	60.2	65.0	51.2
Specificity (%)	82.4	77.9	77.9	85.3	95.6	100

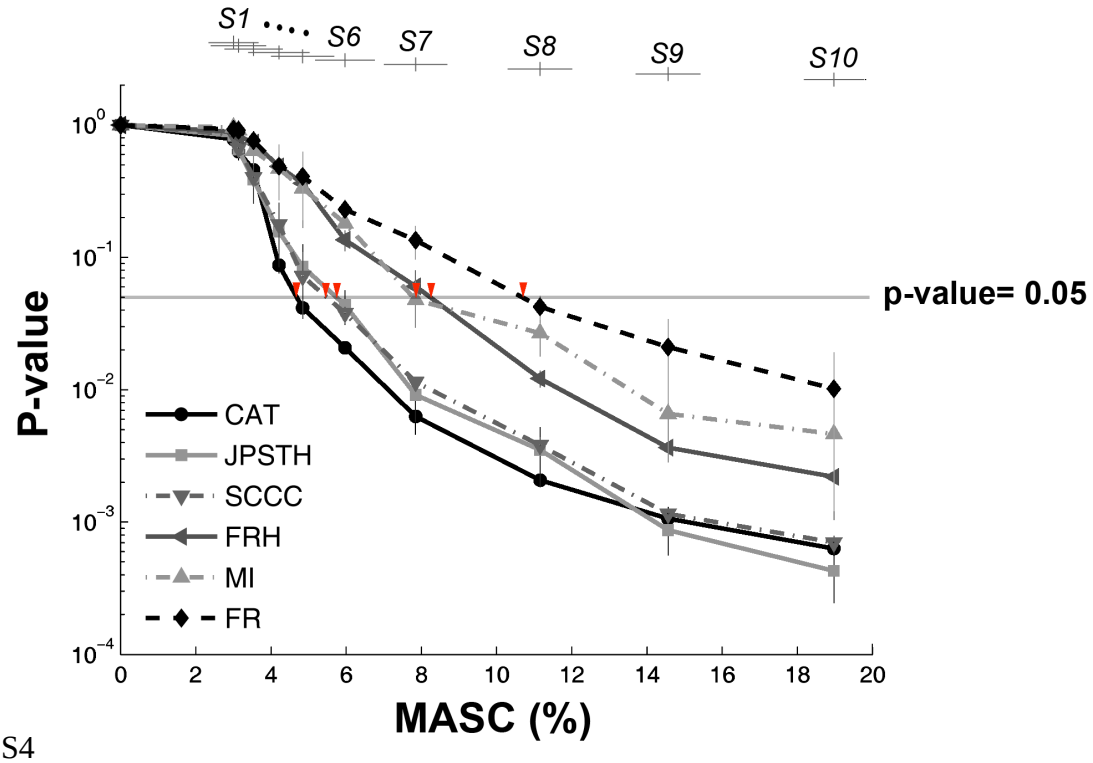

Figure S4

S5: Movies of CATs in a MEA culture: before and after tetanization.

Different patterns of CATs were obtained from evoked responses to different probe electrodes in MEA cultures. Also, CATs from the same probe electrode were found different before and after tetanization (shown **Movie S5a** and **Movie S5b**, respectively). **A.** The rasterplot of 10 seconds of network activity at 60 electrodes. Evoked responses to different probe electrodes are shown in different colors (the same color was used for the same probe electrode in 2 movies). **B.** Activity distribution in 60-channel MEA. Activity intensity at different electrodes is shown by black filled circles with different sizes. The locations of probe electrodes are indicated by crosses with the corresponding colors shown in A. **C.** The corresponding CATs. The color of the trajectory represents the corresponding evoked response shown in A. The scales in the 2 movies are the same. Time is represented in the red bar at the bottom of A.

S6: CATs in all experiments in MEA cultures: before and after tetanization.

Different patterns of CATs were obtained before and after tetanization from 6 experiments in MEAs (see figure). CATs obtained before tetanization (*Pre*) and after tetanization (*Post*) for each probe electrode are shown. The column-row numbers of corresponding probe electrodes are shown in the 8 by 8 MEA grids shown in the middle. The tetanization electrodes are depicted by thick black circles. For each probe, CATs calculated for each "block" (see Methods) are shown in black lines and overlaid. The averaged CATs are shown in colored circles (from blue to red).

092705_A

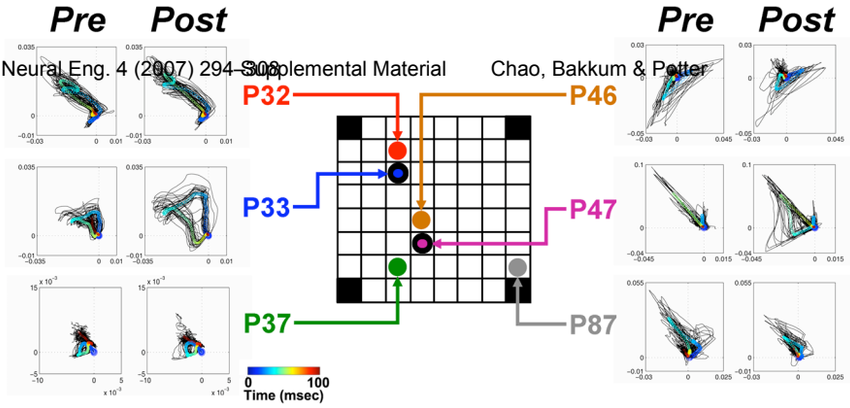

092605_B

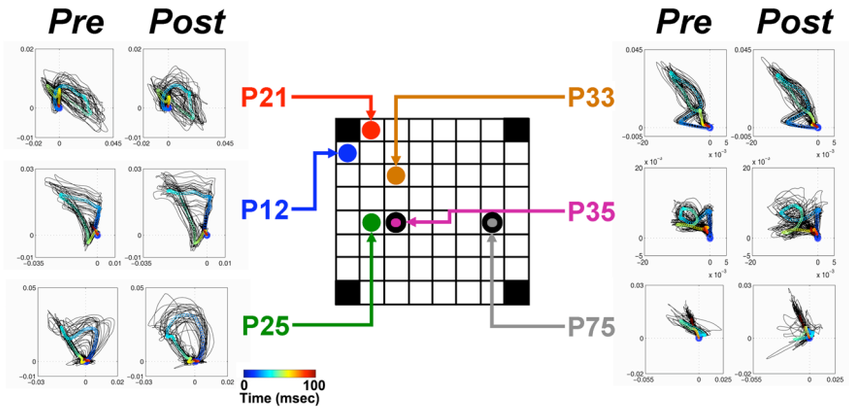

030106_F

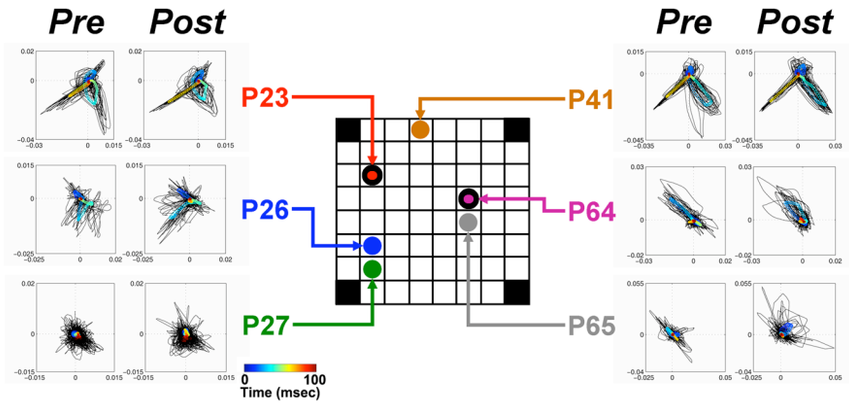

030206_B

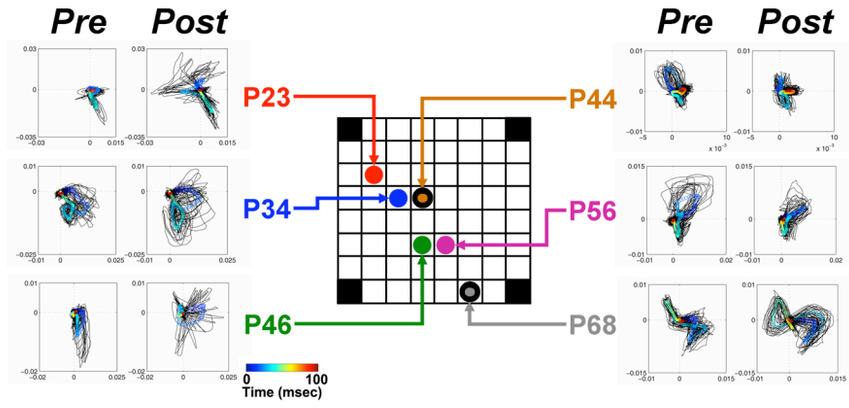

091905_A

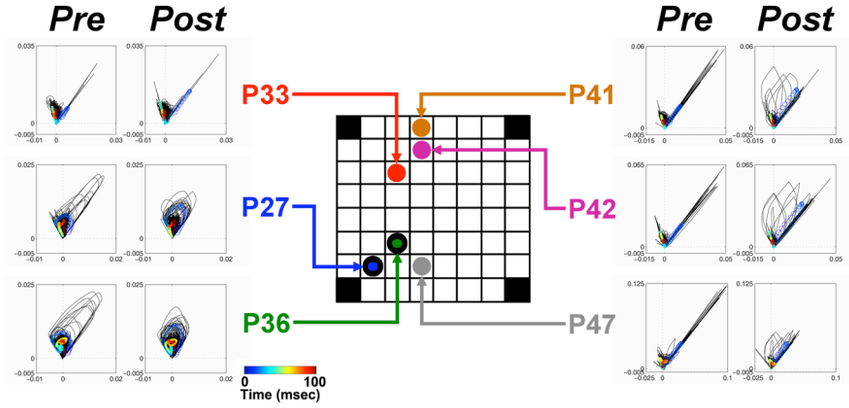

090705_A

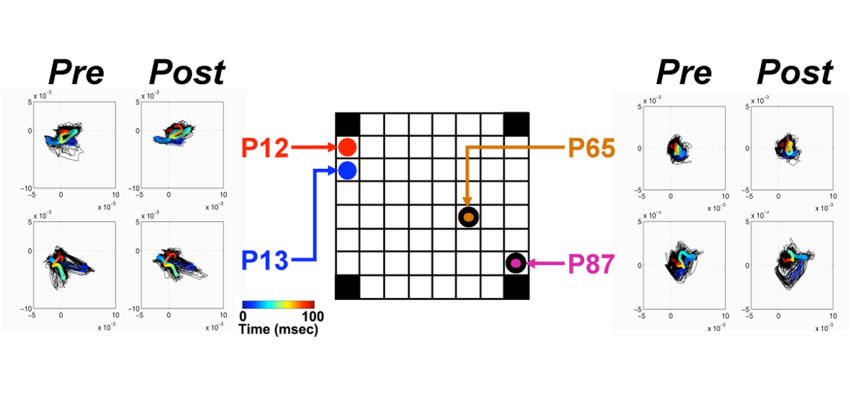

S7: Calculation of center of weights (CW) for simulations.

Plastic changes in the simulated networks' functional architecture can be represented by the trajectory of the center of weights (CW). Let $W_i(t)$ be the weight of synapse i at time t. Let X_i and Y_i indicate the horizontal and vertical distances from the post-synaptic neuron of the synapse i to a reference point (the center of the dish was used). Then, CW of time t is a two dimensional vector:

$$\vec{CW}(t) = \frac{\sum_{i=1}^{N} W_i(t) \cdot [X_i, Y_i]}{\sum_{i=1}^{N} W_i(t)}$$

where N is the total number of excitatory synapses. Note that while CAT describes the spatiotemporal patterns of signal propagation, CW shows the dynamics of connection strengths.

References

Aertsen AM, Gerstein GL, Habib MK, Palm G (1989) Dynamics of neuronal firing correlation: modulation of "effective connectivity". J Neurophysiol 61:900-917.

Brody CD (1999) Correlations Without Synchrony. Neural Computation 11:1537-1551.

Brunel N, Nadal J-P (1998) Mutual Information, Fisher Information, and Population Coding. Neural Computation 10:1731-1757.

Chao ZC, Bakkum DJ, Wagenaar DA, Potter SM (2005) Effects of random external background stimulation on network synaptic stability after tetanization—A modeling study. Neuroinformatics 3:263-280.

Eggermont J (1992) Neural interaction in cat primary auditory cortex. Dependence on recording depth, electrode separation, and age. J Neurophysiol 68:1216-1228.

Franco L, Rolls ET, Aggelopoulos NC, Treves A (2004) The use of decoding to analyze the contribution to the information of the correlations between the firing of simultaneously recorded neurons. Exp Brain Res 155:370-384.

Gerstein G, Perkel D (1969) Simultaneously recorded trains of action potentials: analysis and functional interpretation. Science 164:828-830.

Izhikevich EM, Desai NS (2003) Relating STDP to BCM. Neural Computation 15:1511-1523.

Izhikevich EM, Gally JA, Edelman GM (2004) Spike-Timing Dynamics of Neuronal Groups

Cerebral Cortex 14:933-944.

Kawaguchi H, Fukunishi K (1998) Dendrite classification in rat hippocampal neurons according to signal propagation properties - Observation by multichannel optical recording in cultured neuronal networks. Experimental Brain Research 122:378-392.

Latham PE, Richmond BJ, Nirenberg S, Nelson PG (2000) Intrinsic dynamics in neuronal networks. II. Experiment. Journal of Neurophysiology 83:828-835.

Markram H, Gupta A, Uziel A, Wang Y, Tsodyks M (1998) Information processing with frequency-dependent synaptic connections. Neurobiology of Learning and Memory 70:101-112.

Marom S, Shahaf G (2002) Development, learning and memory in large random networks of cortical neurons: Lessons beyond anatomy. Quarterly Reviews of Biophysics 35:63-87.

Michalski A, Gerstein GL, Czarkowska J, Tarnecki R (1983) Interactions between cat striate cortex neurons. Experimental Brain Research 51:97 - 107.

Moddemeijer R (1989) On Estimation of Entropy and Mutual Information of Continuous Distributions. Signal Processing 16:233-246.

Natschlager T, Markram H, Maass W (2002) Computer models and analysis tools for neural microcircuits. In: A Practical Guide to Neuroscience Databases and Associated Tools.

Paninski L (2003) Estimation of Entropy and Mutual Information. Neural Computation 15:1191-1253.

Segev R, Ben-Jacob E (2000) Generic modeling of chemotactic based self-wiring of neural networks. Neural Networks 13:185-199.

Song S, Miller KD, Abbott LF (2000) Competitive hebbian learning through spike-timing-dependent synaptic plasticity. Nature Neuroscience 3:919-926.

Ventura Vr, Cai C, Kass RE (2005) Trial-to-Trial Variability and Its Effect on Time-Varying Dependency Between Two Neurons. J Neurophysiol 94:2928-2939.